

## Article

# Unique Association of Sulphosalts from the Kľáčianka Occurrence, Nízke Tatry Mts., Slovak Republic

Jiří Sejkora <sup>1,\*</sup>, Martin Števkó <sup>2</sup>, Jaroslav Pršek <sup>3</sup>, Róbert Hovorič <sup>4</sup>, Emil Makovický <sup>5</sup> and Martin Chovan <sup>6</sup>

<sup>1</sup> Department of Mineralogy and Petrology, National Museum, Cirkusová 1740, 193 00 Praha 9—Horní Počernice, Czech Republic

<sup>2</sup> Earth Science Institute, Slovak Academy of Sciences, Dúbravská Cesta 9, 840 05 Bratislava, Slovakia; msminerals@gmail.com

<sup>3</sup> Faculty of Geology, Geophysics and Environmental Protection, AGH-University of Science and Technology, Al. Mickiewicza 30, 30-059 Kraków, Poland; prsek@yahoo.com

<sup>4</sup> Faculty of Natural Sciences, Comenius University, Mlynská Dolina, Ilkovičova 6, 842 15 Bratislava, Slovakia; robert.hovoric@gmail.com

<sup>5</sup> Department of Geoscience and Resource Management, University of Copenhagen, Østervoldgade 10, 1350 Copenhagen, Denmark; emilm@ign.ku.dk

<sup>6</sup> Department of Mineralogy, Petrology and Geology of Mineral Deposits, Comenius University, Ilkovičova 6, 842 15 Bratislava, Slovakia; chovanmmm@gmail.com

\* Correspondence: jiri.sejkora@nm.cz

**Abstract:** Unique association of sulphosalts was discovered at the Kľáčianka occurrence, Nízke Tatry Mts., Slovak Republic. It is bound to thin hydrothermal veins with Sb mineralization hosted by the Variscan muscovite-biotite granodiorite and granite of Prašivá type. Ore mineralogy and crystal chemistry of ore minerals are studied here by ore microscopy, X-ray powder diffraction, electron microprobe analyses, and Raman spectroscopy. The early ore mineralization composed of pyrite and arsenopyrite is hosted in quartz gangue and is followed by abundant association of sulphosalts. Stibnite, zinkenite, robinsonite (including Cu-bearing variety), jamesonite, scainiite, dadsonite, disulfodadsonite, rouxelite, chovanite, semseyite, boulangerite, geocronite, tintinaite (with low Bi contents), tetrahedrite-(Fe), tetrahedrite-(Zn), bournonite, chalcostibite, bismuthinite, and gladite in association with sphalerite and rare galena and gold are identified here. The chlorine-rich character of the described sulphosalt association is its characteristic phenomenon. It is represented not only by the occurrence of Cl-sulphosalt and dadsonite, but increased Cl contents were detected in boulangerite, chovanite, disulfodadsonite, robinsonite, rouxelite, scainiite, or tintinaite. The presence of oxygen-containing sulphosalts, such as rouxelite, scainiite and chovanite, is also interesting. The crystallization of these rare chloro-, oxy- and oxy-chloro-sulphosalts at the Kľáčianka occurrence required very specific conditions (elevated O<sub>2</sub>/S<sub>2</sub> fugacity) and high chlorine activity in ore-forming fluids.

**Keywords:** Sb hydrothermal mineralization; Kľáčianka; Nízke Tatry Mts; Cl-rich sulphosalts; O-rich sulphosalts



check for updates

**Citation:** Sejkora, J.; Števkó, M.; Pršek, J.; Hovorič, R.; Makovický, E.; Chovan, M. Unique Association of Sulphosalts from the Kľáčianka Occurrence, Nízke Tatry Mts., Slovak Republic. *Minerals* **2021**, *11*, 1002. <https://doi.org/10.3390/min11091002>

Academic Editor: Paola Bonazzi

Received: 2 August 2021

Accepted: 9 September 2021

Published: 14 September 2021

**Publisher's Note:** MDPI stays neutral with regard to jurisdictional claims in published maps and institutional affiliations.



**Copyright:** © 2021 by the authors. Licensee MDPI, Basel, Switzerland. This article is an open access article distributed under the terms and conditions of the Creative Commons Attribution (CC BY) license (<https://creativecommons.org/licenses/by/4.0/>).

## 1. Introduction

Sulphosalts, especially lead-antimony ones, are typical accessory ore minerals of the hydrothermal veins with stibnite mineralization in the Nízke Tatry Mts. Zinkenite, robinsonite, boulangerite, jamesonite, chalcostibite, bournonite, and minerals of tetrahedrite group are quite common and are present at the majority of antimony deposits and ore occurrences in the Nízke Tatry Mts. [1–12], whereas other sulphosalts like scainiite, dadsonite, chovanite, rouxelite, bismuthinite derivatives, or kobellite homologues are much more rare. They have so far only been discovered at a limited number of localities [4,7,13–16]. The Kľáčianka ore occurrence, although small, represents a unique locality with a rather complex association of Pb–Sb, Hg, Cl, O, and Cu-bearing sulphosalts.

The first brief mineralogical characterisation of the Kľačianka ore occurrence was done by Jakeš [17], who described the occurrence of stibnite, zinkenite, and tetrahedrite. New mineralogical research started with the unpublished diploma thesis of Bakos [18]. These results were later partly published by Bakos et al. [6]. Using EPMA, arsenopyrite, pyrite, marcasite, sphalerite, galena, stibnite, tetrahedrite, bournonite, chalcocite, jamesonite, zinkenite, robinsonite, *heteromorphite*, boulangerite, and Cu–Pb–Bi (Sb) sulphosalts were identified here. Pršek [7] described the chemical composition of some sulphosalts from Kľačianka in his unpublished extensive Ph.D. thesis: bournonite, boulangerite, *heteromorphite*, probable dadsonite (Cl content was not analysed), jamesonite, *pellouxite* (Cl and Hg contents were not analysed), robinsonite, zinkenite, bismuthinite, and tetrahedrite. These results from the Kľačianka were later partly mentioned in the conference proceedings by Pršek and Ozdín [19] and Chovan et al. [20]. The newest, but also unpublished research was done by Hovorič [21] for his Master thesis. On the basis of EPMA data, he described stibnite, zinkenite, jamesonite, robinsonite, dadsonite, tetrahedrite, chalcocite, scainite, bournonite, rouxelite, *two unknown Pb–Sb sulphosalts*,  $Pb_2Sb_2S_5$  phase, boulangerite, geocronite, Cu–Pb–Bi sulphosalts, and gold. The crystal structure of dadsonite from the Kľačianka occurrence and its chemical composition was published by Makovicky et al. [15]. The crystal structure of a new sulphosalt with the empirical formula  $Pb_{15-2x}Sb_{14+2x}S_{36}O_x$  from Kľačianka was later published by Makovicky and Topa [22]. A complete description of this new mineral phase defined as chovanite was then published by Topa et al. [16] based on samples from Kľačianka as well as Dúbrava and Malé Železné.

The detailed study of unique mineral association of the Kľačianka occurrence with presence of chloro- and oxy-sulphosalts, presented in this paper, is a part of our long-term systematic and detailed mineralogical research focused on sulphosalts from various occurrences. This research is based not only on routine electron microprobe data, but also on the study of minor elements (as Hg, Cu, Cl etc.) in the chemical composition of sulphosalts [23–25], single-crystal X-ray diffraction [16], powder X-ray diffraction [26,27], or Raman spectroscopy [27,28].

## 2. Geological Setting

The small Kľačianka occurrence of hydrothermal Sb mineralization is located in the Kľačianska dolina (Kľačianska valley) situated on the northern slope of the Nízke Tatry Mts., 6.5 km south of the village Liptovské Kľačany near Liptovský Mikuláš, Slovakia. The occurrence is represented by a small main dump partly overgrown by trees and an incision of a fully collapsed adit as well as several smaller pits and short exploration adits located east of the main dump. In the past few years, the main dump was practically fully extracted and its material was used for the construction of local forest roads. Only a small amount of the dump material is still available at the locality. GPS coordinates of the main dump are: 48.975681° N and 19.467352° E, 1105 m a.s.l.

The first written reference to the mining activity in the area of Lúpčianska and Križianska valley dates back to 1753, when Juraj Roman received the permission to dig at the Rišianka and in Kľačianska valley [6]. In the 18th and 19th centuries, intensive mining of Ag and Sb ores was performed in this area with variable results [29]. The Kľačianka occurrence was later studied (not in much detail) during the regional exploration for Sb ores. Unpublished work of Lisý [30], Kubíny [31], Lehotský [32] or Michálek [33] can be mentioned as an example.

The Nízke Tatry Mts. form a 95 km long and 25 km wide E-W trending mountain range located in central Slovakia. They are geologically subdivided by the Čertovica fault line in the western (Ďumbier) and eastern (Kráľová Hoľa) parts. The crystalline basement of the Ďumbier part belongs to the Tatric Superunit and is represented by various types of Variscan granitic rocks (e.g., Ďumbier, Prašivá and Latiborská hoľa type) as well as by metamorphic rocks, mainly ortho- and paragneisses, migmatites, and amphibolites [34–38]. The crystalline basement is overlain by autochthonous to para-autochthonous Mesozoic sedimentary cover rocks (the Tatric Envelope Unit). Two allochthonous Mesozoic units—the

Fatric Unit (Križná nappe) and the Hronic Unit (Choč nappe), occur in a tectonically higher position [34,37]. The Tatric part of the Nízke Tatry Mts. is an important source of metals, especially of Sb, Au, Fe, and Cu, with the two principal and historically most important types of hydrothermal ore mineralization being: veins with Sb ± Au mineralization and siderite-quartz-sulphide veins [4,39–41].

There is a small occurrence of hydrothermal veins with Sb mineralization. Kl'áčianka is located in the Ďumbierske Tatry crystalline complex, essentially in the middle of the joining point of the recently-mined large Dúbrava Sb deposit [41–44] and an important historical Magurka mining district with Sb–Au mineralization [3,40,45]. There are a number of other small occurrences of hydrothermal Sb mineralization in this area (Figure 1), especially Malé Železné, Rišianka [5], Kráмец, and Veľké Oružné [6], as well as occurrences located in L'ubel'ská valley (especially the Dimitrij vein), which are considered as a part of Dúbrava Sb deposit [46]. Ore veins at the Kl'áčianka occurrence are probably of the N-S direction and are up to 1 m thick [32]. They are hosted in the Variscan muscovite-biotite granodiorite and granite of Prašivá type [34,47]. Our field observations suggest the presence of several thinner veins or an irregular stockwork at the studied locality with different mineral parageneses in individual veins.

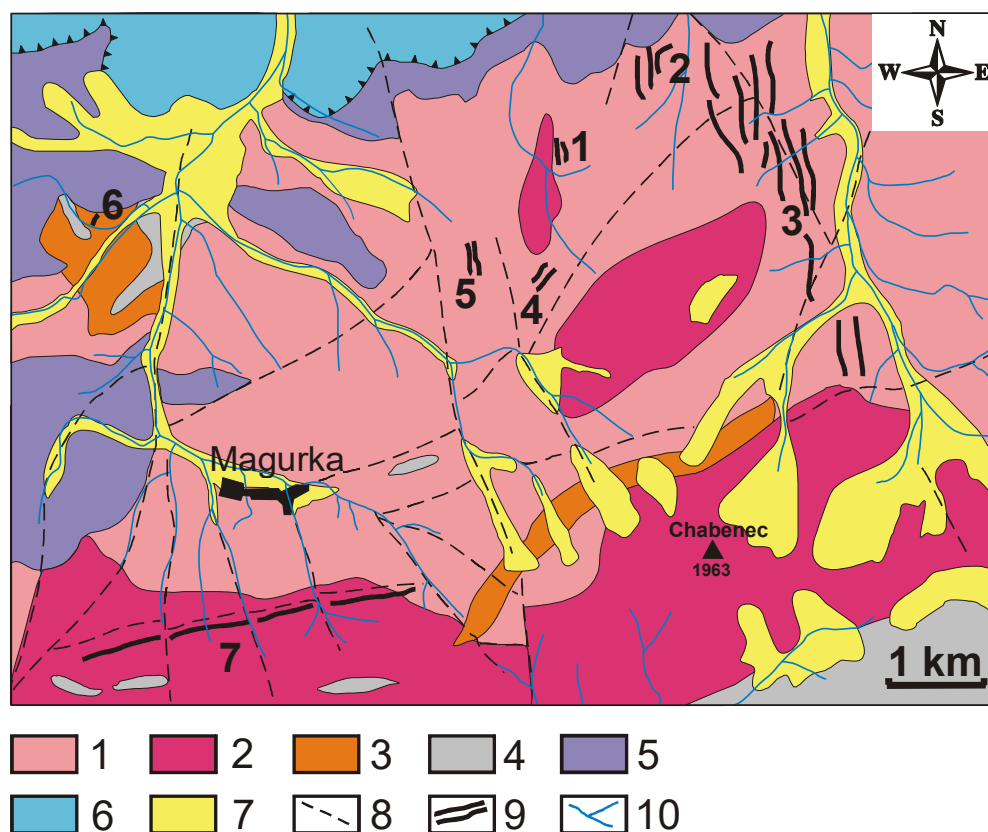


**Figure 1.** Geological map of the northern part of the central section of the Nízke Tatry Mts. (simplified after Biely [34]). Tatric Unit: 1.—granodiorites (Prašivá type), 2.—tonalites to granodiorites (Ďumbier type), 3.—leucocratic granites, 4.—metamorphic rocks (phyllites, paragneisses), 5.—Tatric Envelope Unit (mainly quartzites), 6.—Fatric Unit (dolostones, limestones), 7.—Quaternary sediments, 8.—faults, 9.—ore veins (1—Kl'áčianka occurrence, 2—Dúbrava-L'ubel'ská-Dimitrij vein, 3—Dúbrava Sb deposit, 4—Kráмец occurrence, 5—Rišianka occurrence, 6—Malé Železné occurrence, 7—Magurka Sb–Au deposit), 10.—creeks.

### 3. Experimental Techniques

The mine workings at Kl'áčianka are inaccessible and therefore the studied ore material was collected in 2009–2015 from the preserved mine dumps. Part of the studied material

(massive stibnite/zinkenite mineralization) comes from a system of randomly oriented hydrothermal veins, which was recently uncovered in the roadcut of the newly constructed forest road located 75 m NE from the main dump. These hydrothermal quartz veins are up to 25 cm thick and contain massive lenses of stibnite, sulphosalts (mainly zinkenite), and minor pyrite.

The initial inspection of the samples consisted of rapid phase analysis by means of powder X-ray diffraction (more than 400 individual exposures). Samples for further more detailed research were selected especially on the basis of these results.

The powder X-ray diffraction data (PXRD) of the studied minerals (handpicked samples) were collected on a Bruker D8 Advance diffractometer (National Museum, Prague, Czech Republic) with a solid-state 1D LynxEye detector using monochromatic  $\text{CuK}_{\alpha 1,2}$  radiation and operating at 40 kV and 40 mA. To minimize the complicated shape of the background, the powder samples were placed onto a flat low-background silicon wafer. The powder patterns were collected using Bragg-Brentano geometry in the range  $3\text{--}55^\circ 2\theta$ , in  $0.02^\circ$  steps with a counting time of 1–2 s per step (rapid phase analyses), and  $3\text{--}70^\circ 2\theta$ , in  $0.01^\circ$  steps with a counting time of 20 s per step (for refinement of unit-cell parameters). Positions and intensities of reflections were found and refined using the PearsonVII profile-shape function with the ZDS program package [48] and the unit-cell parameters were refined by the least-squares algorithm implemented by Burnham [49]. The experimental powder XRD patterns were indexed in line with the calculated values of intensities obtained from the published crystal structure information, based on Lazy Pulverix program [50].

Polished sections of the studied samples from Kl'áčianka were prepared for optical investigation, measurement of microhardness, and chemical analysis using standard diamond polishing techniques. Optical properties of minerals in reflected light were observed with a Nikon Eclipse ME600 microscope.

Chemical analyses of individual ore minerals were performed using several electron microprobes operating in the wavelength-dispersive (WDS) mode—Cameca SX 100 at the laboratories of National Museum, Prague, Czech Republic (labelled PR in Supplementary Materials); the same microprobes at State Geological Institute of Dionýz Štúr, Bratislava, Slovakia (labelled BA); and Faculty of Science, Masaryk University, Brno, Czech Republic (labelled BR). Part of the analyses were performed also using a JEOL Superprobe 8600 JXA electron microprobe at the Paris Lodron University, Salzburg, Austria (labelled SA). The analytical conditions, standards, and used X-ray lines are listed in Table S1. Contents of the elements, which are not included in the tables, but were analysed quantitatively, were consistently below the detection limit (ca. 0.03–0.20 wt.% for individual elements). Raw intensities were converted into the concentrations of elements using automatic “PAP” matrix-correction software [51] for Cameca microprobes and on-line ZAF correction procedure for the JEOL microprobe. The results obtained from all laboratories are fully comparable, both for the major and minor elements. The complete set of analyses (more than 1300 individual points) is given as Supplementary Material of this paper.

Raman spectra of selected samples were collected in the range  $3600\text{--}26\text{ cm}^{-1}$  using a DXR dispersive Raman Spectrometer (Thermo Scientific, Waltham, Massachusetts, USA) mounted on a confocal Olympus microscope. The Raman signal was excited by an unpolarised 633 nm He–Ne gas laser and detected by a CCD detector (size  $1650 \times 200$  pixels, Peltier cooled to  $-60^\circ\text{C}$ , quantum efficiency 50%, and dynamic range 360–1100 nm). The experimental parameters were:  $100\times$  objective, 10 s exposure time, 100 exposures,  $50\ \mu\text{m}$  slit spectrograph aperture, and 0.5 mW laser power level. The spectra were repeatedly acquired from different grains in order to obtain a representative spectrum with the best signal-to-noise ratio. The possible thermal damage of the measured point was excluded by visual inspection of the exposed surface after measurement, by observation of possible decay of spectral features in the start of excitation, and checking for thermal downshift of Raman lines. The instrument was set up by a software-controlled calibration procedure using multiple neon emission lines (wavelength calibration), multiple polystyrene Raman bands (laser-frequency calibration), and standardized white-light sources (intensity cal-

ibration). Spectral manipulations were performed using the Omnic 9 software (Thermo Scientific, Waltham, MA, USA).

#### 4. Description of the Ore Mineralization

The studied samples represent fragments of quartz gangue with a subordinate amount of dolomite hosted in hydrothermally altered granitic country rocks. These fragments indicate the presence of irregular veins with thickness reaching up to 20 cm, but usually only 3–5 cm thick. The studied samples show distinct post-deposition tectonic overprint. The sulphosalts occur as aggregates that reach locally up to 10 cm, but usually only 0.1–1 cm in size. The fine impregnations of sulphosalts as well as base-metal sulphides (pyrite, arsenopyrite, sphalerite) in hydrothermally altered granites were also observed.

##### 4.1. Pb–Sb Sulphosalts

**Zinkenite** occurs generally in a close association with stibnite, and this assemblage is one of the most abundant in the studied ore material. It forms fibrous to fine-grained aggregates up to 10 cm in size. In polished sections, zinkenite forms relic aggregates up to 1 mm or abundant, irregularly dispersed round to elongated inclusions ranging in size from a few  $\mu\text{m}$  to 100–150  $\mu\text{m}$  enclosed in younger stibnite (Figure 2a). It is also occasionally replaced by jamesonite and scainiite (Figure 2b). The PXRD data of zinkenite from Kľačianka agree very well with published data of this mineral phase and also with the theoretical pattern calculated from the crystal structure information published by Portheine, Nowacki [52] and average structural data of Biagioni et al. [53]; its refined unit-cell parameters are given in Table 1. For zinkenite, the ideal formula  $\text{Pb}_9\text{Sb}_{22}\text{S}_{42}$  is given in literature [54], but the presence of minor amounts of Cu is characteristic for samples from the several worldwide localities and the substitution mechanism  $\text{Sb}^{3+} + \square \rightarrow \text{Pb}^{2+} + \text{Cu}^+$  has been proposed, with  $\text{Cu}^+$  filling an empty tetrahedral site close to the pseudo-hexagonal axis [53,55]. During the study of chemical composition of zinkenite from Kľačianka (Table S2), we observed Cu contents in the range 0.22–0.64 *apfu* and locally also minor amounts of Ag (reaching up to 0.18 *apfu*). Similar contents of Cu or Ag were described in zinkenite from Saint Pons, France—0.7 *apfu* Cu [53]; Sentyabr'sky prospect, Chukotka—0.27–1.17 *apfu* Cu up to 0.45 *apfu* Ag [56]; or Slovak localities Lomnistá and Husárka—0.27–0.33 *apfu* Cu, up to 0.11 *apfu* Ag [12]. The mean composition of studied zinkenite (calculated from 81 analyses on the basis of 73 *apfu*) is  $(\text{Cu}_{0.37}\text{Ag}_{0.08})_{\Sigma 0.45}\text{Pb}_{9.12}\text{Sb}_{21.64}\text{S}_{41.80}$ .

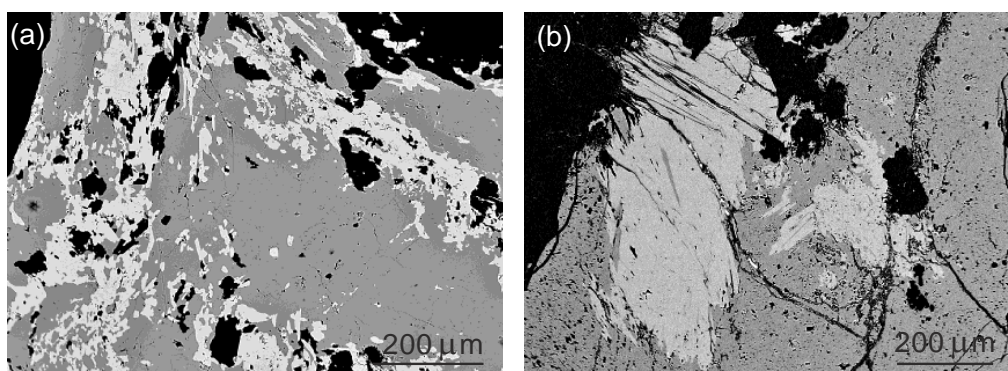


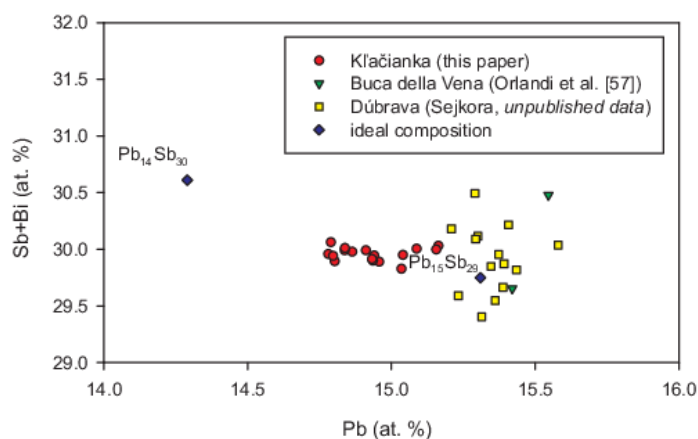
**Figure 2.** (a) Abundant, irregularly dispersed round to elongated inclusions of zinkenite (white) in stibnite (grey); (b) scainiite aggregates (light grey) in earlier aggregates of zinkenite (dark grey). BSE photos.

**Table 1.** Unit-cell parameters for selected sulphosalts from Kľáčianka refined from PXRD.

|                   | SG                                 | <i>a</i> [Å] | <i>b</i> [Å] | <i>c</i> [Å] | $\beta$ [°] | <i>V</i> [Å <sup>3</sup> ] |
|-------------------|------------------------------------|--------------|--------------|--------------|-------------|----------------------------|
| zinkenite         | <i>P</i> 6 <sub>3</sub>            | 22.1413 (9)  |              | 4.3286 (4)   |             | 1837.74 (17)               |
| robinsonite       | <i>I</i> 2/ <i>m</i>               | 23.634 (3)   | 3.9773 (9)   | 24.412 (3)   | 93.76 (1)   | 2289.7 (6)                 |
| jamesonite        | <i>P</i> 2 <sub>1</sub> / <i>c</i> | 4.0232 (12)  | 19.107 (3)   | 15.722 (3)   | 91.88 (2)   | 1207.9 (3)                 |
| boulangerite      | <i>P</i> 2 <sub>1</sub> / <i>a</i> | 21.556 (3)   | 23.479 (4)   | 8.075 (2)    | 100.79 (1)  | 4014.7 (1.3)               |
| stibnite          | <i>Pnma</i>                        | 10.3115 (8)  | 3.8382 (3)   | 11.2286 (9)  |             | 487.50 (5)                 |
| chalcocite        | <i>Pnma</i>                        | 6.0223 (4)   | 3.7994 (3)   | 14.5041 (8)  |             | 331.87 (3)                 |
| tetrahedrite-(Zn) | <i>I</i> -43 <i>m</i>              | 10.39911 (8) |              |              |             | 1124.57 (3)                |

SG—space group.

**Scainiite** is rare in the studied mineral association. It forms aggregates and subhedral grains up to 400–500  $\mu\text{m}$  enclosed in aggregates of zinkenite (Figure 2b). Chemical composition of scainiite from Kľáčianka occurrence is close to data published for scainiite from the type locality in Buca della Vena mine, Italy [57] and its abundant occurrence at Dimitrij vein, Dúbrava, Slovakia (Sejkora, unpublished data). Crystal structure study of scainiite from type locality gives the structural formula  $\text{Pb}_{14}\text{Sb}_{30}\text{S}_{54}\text{O}_5$  [58], but this formula has a Pb/Sb ratio ( $\text{Pb}_{14}\text{Sb}_{30}$ ) significantly lower than those obtained by chemical analyses (close to  $\text{Pb}_{15}\text{Sb}_{29}$ ) of scainiite from all known occurrences (Figure 3). This discrepancy between the microprobe and crystallographic data remains unexplained [57]. The ideal formula of scainiite contains five oxygen atoms, but this low O content (0.96 wt.% according to the crystallographic study of Moëlo et al. [58]) cannot be measured precisely with an EPM [57] due to presence of an oxidation film on the surface of the samples [14,57,59]. Unlike samples from the type locality, scainiite from Kľáčianka contains minor contents of Cl up to 0.14 apfu; similar contents were also detected in samples from Dúbrava (0.17–0.33 apfu; Sejkora, unpublished data) or Kremnica deposit (up to 0.19 apfu [24]). The chemical analyses of scainiite and corresponding empirical formulae are given in Table S3.

**Figure 3.** Chemical composition of scainiite in the graph Pb vs. Sb + Bi (at.%).

**Jamesonite** was found as relatively abundant metallic grey fibrous aggregates up to 0.5 cm embedded in quartz gangue. In polished sections, it forms subhedral lath-like or anhedral fine-grained aggregates up to 1 mm in size, partly intergrown with galena and overgrown by subhedral crystals of boulangerite. It was also observed as short lath-like crystals and tiny inclusions enclosed in the earlier robinsonite (Figure 4a). Jamesonite is usually replaced by younger dadsonite and rouxelite. The PXRD data of jamesonite from Kľáčianka agree well with the published data of this mineral phase and also with a theoretical pattern calculated from the crystal structure information published by Léone et al. [60]; its refined unit-cell parameters are given in Table 1. Chemical composition of jamesonite from Kľáčianka (Table S4) corresponds very well to the ideal formula  $\text{FePb}_4\text{Sb}_6\text{S}_{14}$  [54]; only

minor contents of Cu (up to 0.06 *apfu*) were found. The mean composition of jamesonite (calculated from 68 analyses on the base of 25 *apfu*) is  $(\text{Fe}_{0.91}\text{Cu}_{0.03})_{\Sigma 0.94}\text{Pb}_{3.93}\text{Sb}_{6.08}\text{S}_{14.05}$ .

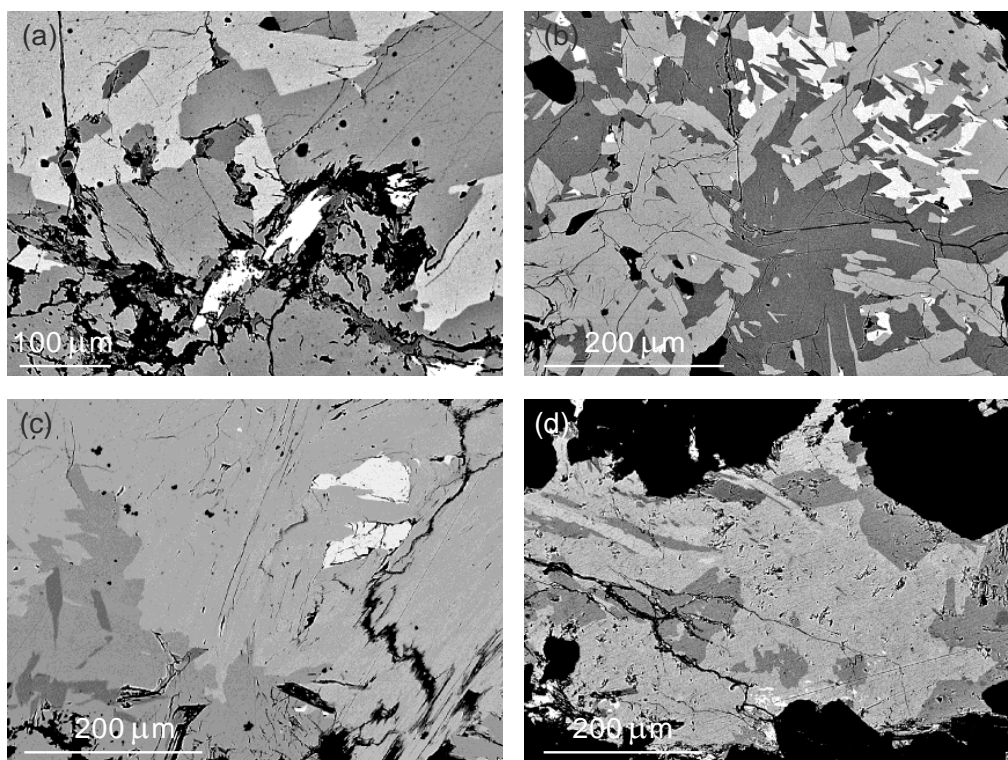


**Figure 4.** (a) The elongated euhedral to subhedral grains of semseyite (white) in fissures of zinkenite aggregates (dark); in association with robinsonite (lighter grey) and jamesonite (darker grey); (b) dadsonite metacrysts (grey) replaced earlier boulangerite (white) and robinsonite (dark); (c) rouxelite aggregates (light grey) with relics of boulangerite (white) replaced earlier robinsonite (dark grey) with jamesonite metacrysts (dark); (d) disulfodadsonite aggregates (grey) in association with earlier robinsonite (dark grey), chovanite (lighter grey), and with relics of boulangerite (white). BSE photos.

**Robinsonite** was found as grey fine-grained aggregates up to 1 cm in size, sometimes with visible fibrous structure, enclosed in quartz gangue. In polished sections, it forms irregular aggregates up to 400–750  $\mu\text{m}$  partly replaced by younger rouxelite, boulangerite, and lath-like crystals of jamesonite (Figure 4a–c) or chovanite and disulfodadsonite (Figure 4d). Together with rouxelite, it is overgrown by dadsonite. The PXRD data of robinsonite from Kl'áčianka agree well with the published data for this mineral phase and also with the theoretical pattern calculated from the crystal structure information published by Makovicky et al. [61]. The refined unit-cell parameters of robinsonite from Kl'áčianka are given in Table 1. Chemical analyses of robinsonite (Table S5) correspond to ideal formula  $\text{Pb}_4\text{Sb}_6\text{S}_{13}$  [54]; determined Pb/Sb ratio ranges between 0.65 to 0.69, which is consistent with the range 0.65–0.73 published for natural robinsonite [62]. Remarkable are the minor contents of Cl up to 0.07 *apfu* (0.13 wt.%); similar contents (up to 0.09 wt.% Cl) were published by Števkó and Sejkora [63] for robinsonite from Čížko baňa occurrence near Ochtiná, Slovakia. Its mean composition (calculated from 72 analyses on the base of 23 *apfu*) is  $\text{Pb}_{3.99}\text{Sb}_{5.99}\text{S}_{12.98}\text{Cl}_{0.04}$ .

Anomalous **Cu-bearing robinsonite** occurs as oval to elongated inclusions up to 30  $\mu\text{m}$  in size in bournonite or irregular to elongated grains up to 100  $\mu\text{m}$  in length in association with bournonite (Figure 5a) and tintinaite in tetrahedrite aggregates. The determined Pb and (Sb + Bi) contents (Table S5) correspond to robinsonite and are clearly different from associated tintinaite (Figure 6); its Pb/(Sb + Bi) ratio (0.66–0.70) is also comparable to robinsonite [62]. The observed minor Bi contents (up to 0.30 *apfu*) are typical

and similar amounts of Bi were reported by Števkó and Sejkora [63] in samples from Ochtiná—Čižko baňa (0.52 *apfu* of Bi); Števkó and Sejkora [25] from Gemerská Poloma (up to 2.08 *apfu* of Bi); and Jambor and Lachance [64] in robinsonite from Salmo (2.35 *apfu* of Bi). The detected minor Cu contents (0.05–0.42 *apfu*) are very unusual for robinsonite as according to Makovický et al. [61], this mineral usually does not contain any other cations (such as Cu, Fe, or Ag) in its crystal structure. The empirical formula of Cu-bearing robinsonite from Kl'áčianka, calculated from 65 analyses on the basis of 23 *apfu*, is  $\text{Pb}_{4.02}\text{Cu}_{0.18}(\text{Sb}_{5.87}\text{Bi}_{0.07})_{\Sigma 5.94}\text{S}_{12.80}\text{Cl}_{0.07}$ .

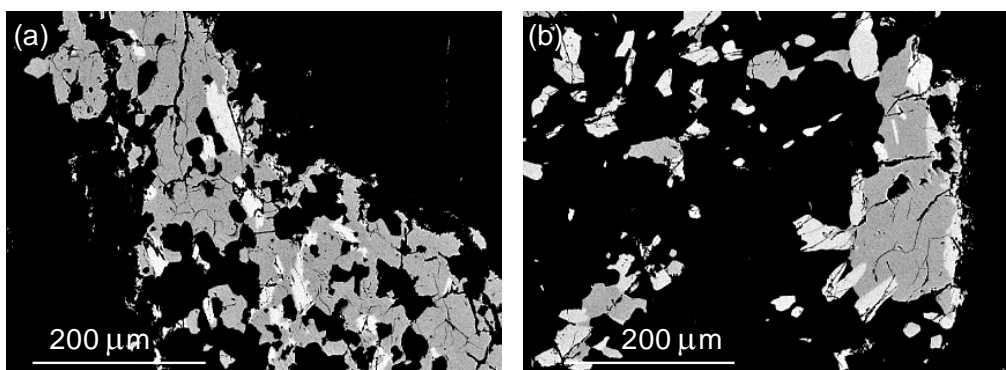


**Figure 5.** (a) The elongated grains of Cu-bearing robinsonite (white) and bournonite aggregates (grey) in tetrahedrite (black); (b) tintinaite grains (white) and bournonite aggregates (grey) in tetrahedrite (black). BSE photos.

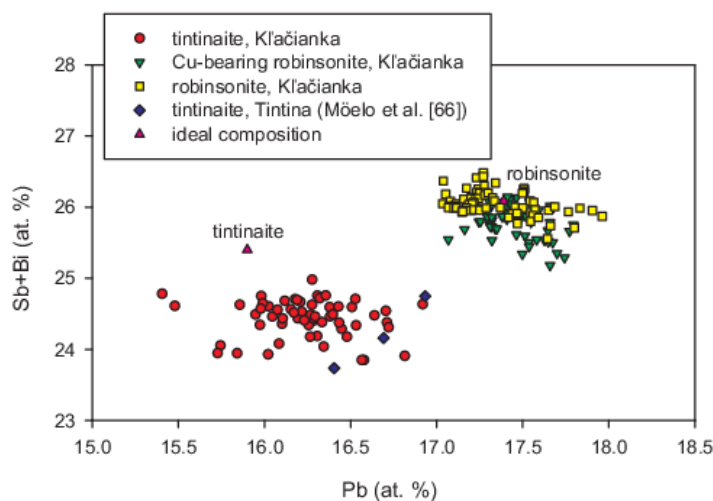


**Figure 6.** Chemical composition of robinsonite and tintinaite in the graph Pb vs. Sb + Bi (at.%); theoretical composition: robinsonite  $\text{Pb}_4\text{Sb}_6\text{S}_{13}$ ; tintinaite  $\text{Pb}_{10}\text{Cu}_2(\text{Sb,Bi})_{16}\text{S}_{35}$ .

**Tintinaite** was found as euhedral acicular crystals up to 100  $\mu\text{m}$  in length enclosed in tetrahedrite or as elongated subhedral grains up to 100  $\mu\text{m}$  in size in association with bournonite and Cu-bearing robinsonite in tetrahedrite aggregates (Figure 5b). The chemical analyses of tintinaite from Kl'áčianka agree well with the composition of members of kobellite-tintinaite homologous series  $\text{Pb}_{10}(\text{Cu,Fe})_2(\text{Sb,Bi})_{16}\text{S}_{35}$ . The order numbers ( $N$ ) for this series were calculated using the formula proposed by Zakrzewski and Makovický [65]:  $N = x(6M^{2+} + 3M^{3+}) / (4M^{3+} - M^{2+}) + (1 - x)(5M^{2+} + 2M^{3+}) / (4M^{3+} - M^{2+})$ , where  $x = T^+ / (T^+ + T^{2+})$ ;  $(1 - x) = T^{2+} / (T^+ + T^{2+})$ ;  $T^+$  is the content of the monovalent tetrahedrally coordinated cations (Cu);  $T^{2+}$  is the content of divalent tetrahedrally coordinated cations (Fe);  $M^{2+}$  is the sum of divalent “large” cations (Pb + Hg); and  $M^{3+}$  is the sum of trivalent “large” cations (Sb + Bi). The silver content was subtracted according to the lillianite-type substitution  $\text{Ag}^+ + \text{Bi}^{3+} = 2\text{Pb}^{2+}$  [26,65]. The calculated number  $N$  ranges

between 2.06 to 2.21 (mean 2.13) and corresponds to the ideal value of 2 given for minerals of tintinaite-kobellite series. The predominant trivalent cation is Sb (with contents 12.96–15.24 *apfu*) and it is only slightly substituted by 0.01–2.45 *apfu* of Bi. Such low Bi contents in tintinaite are uncommon and are so far reported only from the type locality Tintina [66] and occurrence at the Sredni Golgotai [67]; the minimum Bi contents in tintinaite from the nearby Dúbrava antimony deposit are in the 3.74–3.77 *apfu* range [7,43]. The sum of tetrahedrally coordinated cations, Cu and Fe (1.99–3.25 *apfu*), is usually higher than the theoretical value of 2 *apfu* [65,66]; similar excess was also observed at numerous worldwide localities of Sb-rich members [7,68]. The minor contents of Ag, Hg, and Cl were also determined (reaching up to 0.17, 0.32, and 0.51 *apfu*, respectively). The chemical analyses of tintinaite and corresponding empirical formulae are given in Table S6.

**Disulfodadsonite** occurs as rare aggregates up to 500  $\mu\text{m}$  in size in association with earlier robinsonite and chovanite and with relics of boulangerite (Figure 4d). Chemical composition of disulfodadsonite from Kľačianka (Table S7) corresponds well to the ideal formula  $\text{Pb}_{22}\text{Sb}_{26}\text{S}_{60}\text{S}_2$  proposed by Orlandi et al. [69]. In contrast with the type material from Ceragiola in Italy [69], studied disulfodadsonite from Kľačianka contains increased amounts of Cl ranging between 0.11 and 0.50 *apfu* (Figure 7). Its mean composition (calculated from 39 analyses on the base of 110 *apfu*) is  $\text{Pb}_{22.08}\text{Sb}_{26.21}\text{S}_{60}(\text{S}_{1.39}\text{Cl}_{0.32})_{\Sigma 1.71}$ . Due to the similarity of ideal chemical composition of disulfodadsonite and heteromorphite (Figure 8), its determination was confirmed by Raman spectroscopy. The experimental spectrum of disulfodadsonite from Kľačianka (Figure 9) corresponds very well with Raman spectrum of the holotype sample of disulfodadsonite from Ceragiola, Italy.

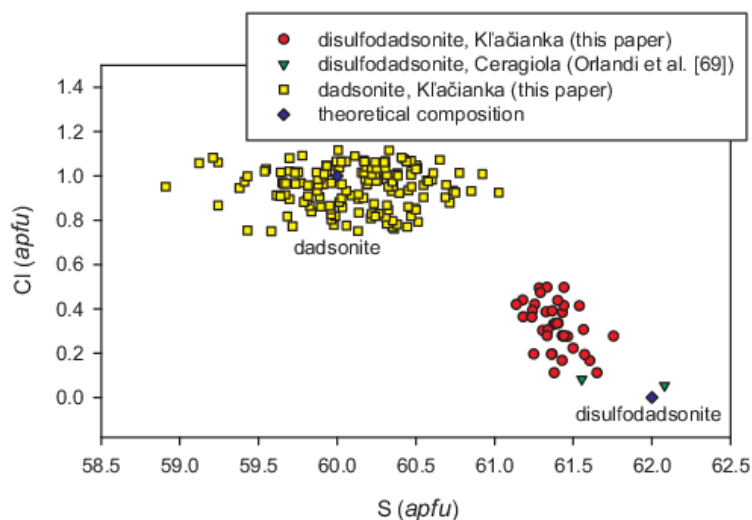


**Figure 7.** Chemical composition of disulfodadsonite and dadsonite in the graph S vs. Cl (at.%); theoretical composition: disulfodadsonite  $\text{Pb}_{22}\text{Sb}_{26}\text{S}_{60}\text{S}_2$ ; dadsonite  $\text{Pb}_{23}\text{Sb}_{25}\text{S}_{60}\text{Cl}$ .

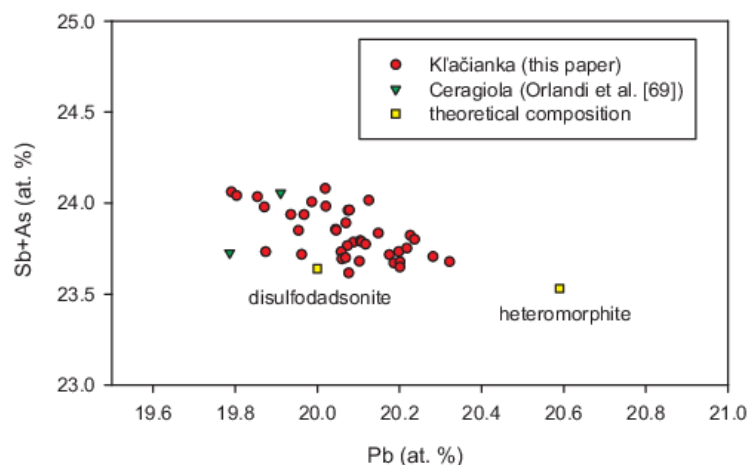


**Figure 8.** Chemical composition of disulfodadsonite in the graph Pb vs. Sb + As (at.%); theoretical composition: disulfodadsonite  $Pb_{11}Sb_{13}S_{30}S$ ; heteromorphite  $Pb_7Sb_8S_{19}$ .

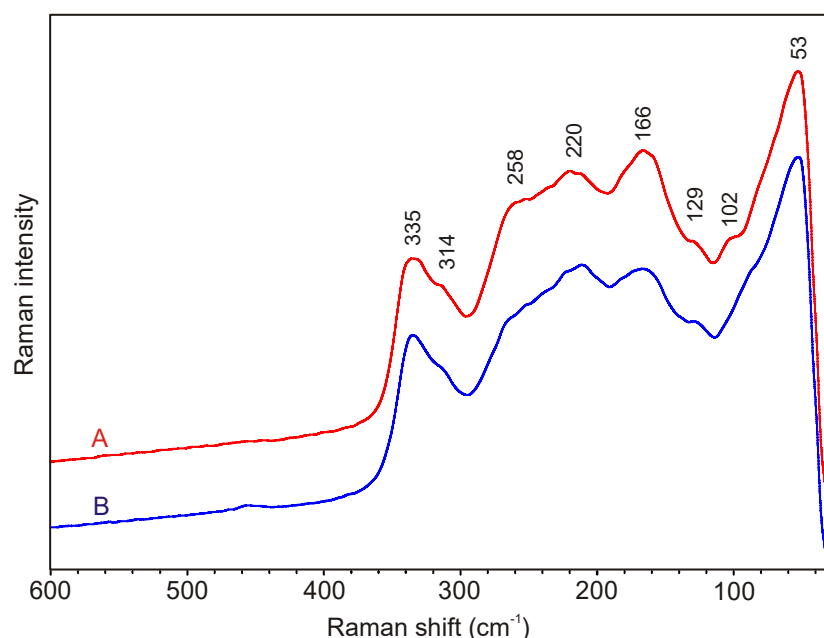


**Figure 9.** Comparison of Raman spectra of disulfodadsonite from Klačianka (A) and Ceragiola, Italy (B).

**Dadsonite** was found as light grey fibrous aggregates with metallic lustre up to 3 cm in quartz gangue; similar aggregates up to 1 cm represented by intergrowths of dadsonite and rouxelite were also observed. It is associated with boulangerite, jamesonite, robinsonite, chovanite, and galena or bournonite. In polished sections, it forms euhedral to subhedral lath-like crystals up to  $25 \times 200 \mu\text{m}$  in size in association with other sulphosalts (Figure 10a) or metacrystals in aggregates of boulangerite and bournonite (Figure 10b). Dadsonite replaces earlier robinsonite and especially rouxelite, which forms irregular relics enclosed in dadsonite (Figure 10c,d). The PXRD data of dadsonite from Klačianka agree well with published data [70,71] and also with theoretical pattern calculated from the crystal structure information published by Makovicky et al. [15]. The obtained experimental PXRD pattern is more complete and more precise than previously published data and, therefore, the complete indexed pattern is given in Table S8. The refined unit-cell parameters of dadsonite from Klačianka are compared in the Table 2 with published data for this mineral phase. Chemical composition of dadsonite from Klačianka (Table S9) corresponds very well to the ideal empirical formula  $Pb_{23}Sb_{25}S_{60}Cl$  [70,72] with determined Cl contents

in the range 0.75–1.12 *apfu* (Figure 7). Its empirical formula (mean of 158 analyses) can be expressed on the basis of 109 *apfu* as  $\text{Pb}_{22.64}\text{Sb}_{25.30}\text{S}_{60.11}\text{Cl}_{0.95}$ , and it is similar to the empirical formula  $\text{Pb}_{23.07}\text{Sb}_{25.10}\text{S}_{59.77}\text{Cl}_{1.05}$  given for dadsonite from Kľačianka used by Makovicky et al. [15] for the single-crystal study.

**Table 2.** Unit-cell parameters of dadsonite (for triclinic space group *P*-1).

|                            | Kľačianka    |                                    | Kľačianka                          |
|----------------------------|--------------|------------------------------------|------------------------------------|
|                            | This Paper   | Makovicky et al. [15] <sup>1</sup> | Makovicky et al. [15] <sup>2</sup> |
| <i>a</i> [Å]               | 8.2734 (14)  | 8.276 (2)                          | 4.1382 (9)                         |
| <i>b</i> [Å]               | 17.3938 (17) | 17.392 (4)                         | 17.394 (4)                         |
| <i>c</i> [Å]               | 19.516 (2)   | 19.505 (4)                         | 19.071 (4)                         |
| $\alpha$ [°]               | 83.512 (10)  | 83.527 (7)                         | 96.442 (7)                         |
| $\beta$ [°]                | 77.866 (13)  | 77.882 (8)                         | 90.113 (8)                         |
| $\gamma$ [°]               | 89.205 (13)  | 89.125 (8)                         | 90.775 (7)                         |
| <i>V</i> [Å <sup>3</sup> ] | 2728.0 (6)   | 2727.2 (9)                         | 1364.0 (5)                         |

<sup>1</sup> 8 Å-refinement; <sup>2</sup> 4 Å-refinement.

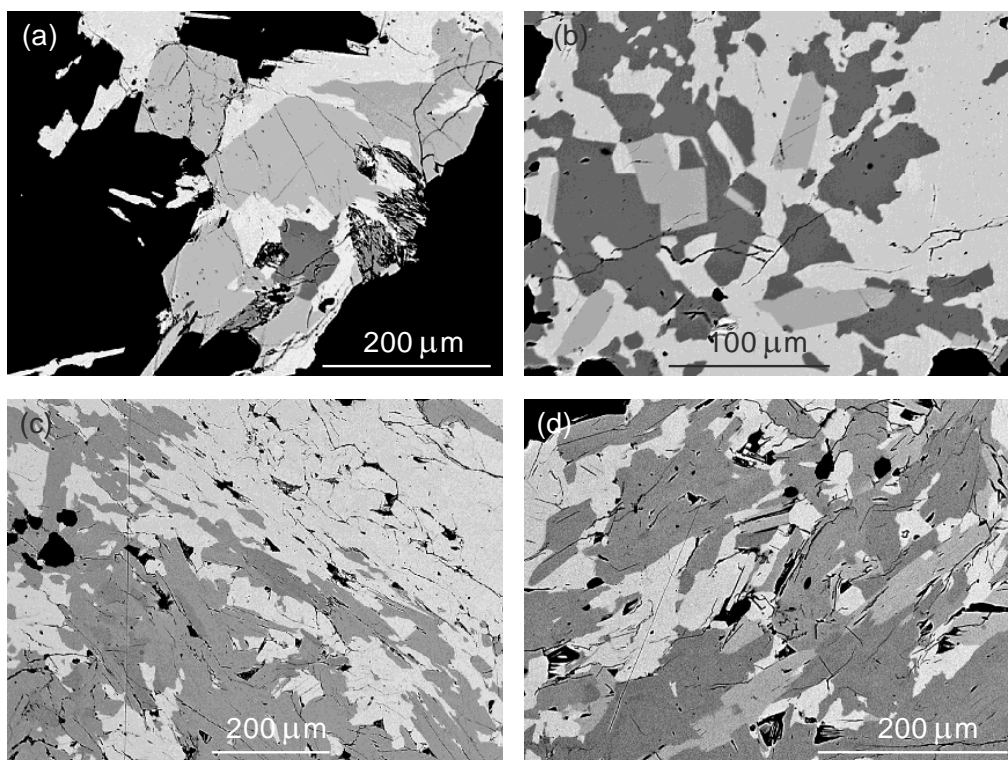


**Figure 10.** (a) Dadsonite (lighter grey) and rouxelite grains (darker grey) in boulangerite (white) with bournonite inclusion (dark); (b) the euhedral metacrysts of dadsonite (grey) in boulangerite (light) and bournonite (dark); (c) the relics of rouxelite (darker grey) in dadsonite aggregates (lighter grey) in association with boulangerite (white); (d) chovanite metacrysts (light grey) in dadsonite (lighter grey)—rouxelite (darker grey) aggregates with earlier boulangerite (white). BSE photos.

**Rouxelite** occurs as rare irregular silvery grey, metallic, fibrous aggregates up to 2 cm in quartz gangue and as light grey aggregates up to 1 cm together with dadsonite, boulangerite, and other sulphosalts. In polished sections, it forms anhedral grains up to 200  $\mu\text{m}$  in size, enclosed in earlier boulangerite (Figure 10a), or intergrows with younger dadsonite (Figure 10c) and chovanite (Figure 10d). Aggregates of rouxelite up to 1 mm in size replace earlier robinsonite and lath-like metacrystals of jamesonite (Figure 4c). The PXRD data of rouxelite from Kľačianka agree with the published data of this mineral phase [14,73] and also with the theoretical pattern calculated from the crystal structure

information published by Orlandi et al. [14]. Due to the fact that in the experimental PXRD pattern of rouxelite from Kľačianka, a significantly larger number of diffraction maxima was observed than previously reported [14]; a complete indexed pattern is given in Table S10. The unit-cell parameters of rouxelite refined from X-ray powder pattern are compared in Table 3 with published data of this mineral phase. Chemical composition of rouxelite from Kľačianka (Table S11) in basic features corresponds to the ideal formula  $\text{Cu}_2\text{HgPb}_{22}\text{Sb}_{28}\text{S}_{64}(\text{O},\text{S})_2$  proposed by Orlandi et al. [14]. The Pb(+Tl) and Sb(+Bi,As) contents are distinctly negatively correlated (Figure 11). Samples from Buca della Vena, Magurka [14], Gemerská Poloma [25], and Kľačianka on average fit to the Pb:Sb ratio of 23:27 and differ from the ratio given by crystal structure study [14] as 22:28. This discrepancy is probably related to the insufficient quality of the resolution of the crystal structure data ( $R = 0.169$ ; [14]), where the occupancy of one mixed (Pb,Sb) position and the three Pb,Sb paired positions was refined. The different Pb:Sb ratios observed in Tl-bearing rouxelite from Monte Arsiccio mine (Figure 11) could be explained by the existence of heterovalent substitutions  $2\text{Pb}^{2+} = \text{Sb}^{3+} + \text{Tl}^+$ ;  $\text{Hg}^{2+} + \text{Pb}^{2+} = (\text{Ag}, \text{Cu})^+ + \text{Sb}^{3+}$ ; and  $2\text{Pb}^{2+} = \text{Sb}^{3+} + \text{Ag}^+$  [73]. The determined Cu contents (mean 2.00, range 1.89–2.11 *apfu*) fit to the ideal ratio of the structural formula. A negative correlation was found between Ag and Hg (Figure 12); substitution of Hg by Ag must be compensated by an equivalent substitution of Pb by Sb, according to the substitution reaction  $\text{Hg}^{2+} + \text{Pb}^{2+} = \text{Ag}^+ + \text{Sb}^{3+}$  [73]. The rouxelite ideal formula contains a mixed (O,S) position, but the very low O content (0.20 wt.% in the type sample) cannot be measured precisely with an EPM [14] due to presence of an oxidation film on the surface of the samples [14,57,59]. Moreover, the uncertainty on the S ratio in the four structural sites does not allow calculation of O ratio by difference on the basis of 66 anions. Remarkable are also the minor contents of Cl in rouxelite from Kľačianka (reaching up to 0.30 *apfu*, 0.10 wt.%) not yet reported for this mineral species; determined Cl contents do not correlate with any other chemical element.

**Table 3.** Unit-cell parameters of rouxelite (for monoclinic space group  $C2/m$ ).

|                       | Kľačianka  | Buca Della Vena       | Monte Arsiccio Mine    |
|-----------------------|------------|-----------------------|------------------------|
|                       | This Paper | Orlandi et al. (2005) | Biagioni et al. (2014) |
| $a$ [Å]               | 43.077 (7) | 43.113 (9)            | 43.10 (2)              |
| $b$ [Å]               | 4.0579 (7) | 4.0591 (8)            | 4.060 (2)              |
| $c$ [Å]               | 37.844 (6) | 37.874 (8)            | 37.88 (2)              |
| $\beta$ [°]           | 117.33 (1) | 117.35 (3)            | 117.33 (2)             |
| $V$ [Å <sup>3</sup> ] | 5877 (2)   | 5887 (2)              | 5889 (5)               |

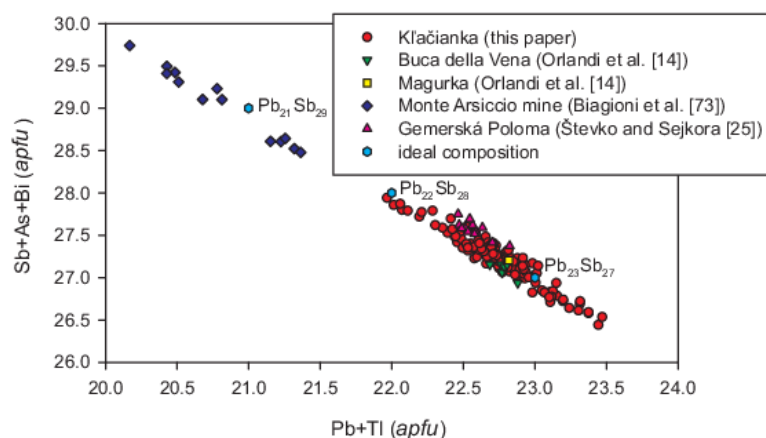


**Figure 11.** Chemical composition of rouxelite in the graph Pb + Tl vs. Sb + As + Bi (*apfu*).

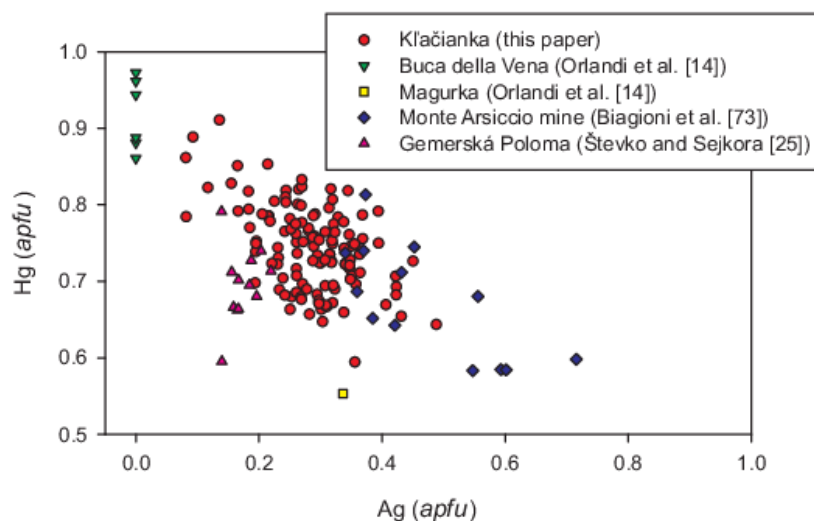


**Figure 12.** Chemical composition of rouxelite in the graph Ag vs. Hg (*apfu*).

**Chovanite** formed rare lath-like metacrystals with sizes from  $40 \times 250$  up to  $150 \times 400 \mu\text{m}$  (Figure 13) enclosed in earlier dadsonite–rouxelite aggregates (Figure 10d); often it selectively replaced rouxelite. It was also observed as relics up to  $200 \mu\text{m}$  in size in aggregates of disulfodadsonite (Figure 4d). The ideal formula  $\text{Pb}_{15-2x}\text{Sb}_{14+2x}\text{S}_{36}\text{O}_x$  ( $x = 0.2$ ) with Pb/Sb ratio about 1.01 was originally proposed for chovanite based on the study of samples from Slovak occurrences Dúbrava, Malé Železné, and Kľačianka [16,22]. Later, Biagioni and Moëlo [74] defined, for Tl-containing chovanite from Italian localities Monte Arsiccio and Pollone mines, the O-rich end-member composition  $\text{Pb}_{28}\text{Sb}_{30}\text{S}_{72}\text{O}$  (or  $\text{Pb}_{14}\text{Sb}_{15}\text{S}_{36}\text{O}_{0.5}$ ) with a Pb/Sb ratio of 0.93. New studies of PXRD confirmed that chovanite samples from Dúbrava deposit (Sejkora, *unpublished data*) indicate Pb/Sb ratio in the range 0.89–0.92 (mean 0.90). When we used the general formula  $\text{Pb}_{15-2x}\text{Sb}_{14+2x}\text{S}_{36}\text{O}_x$ , the  $x$ -value for the samples studied by Topa et al. [16] was 0.06–0.51; for Italian samples [74], the  $x$  value ranged between 0.54 to 0.60 and for new samples of chovanite from Dúbrava the range was 0.89–0.92. During the study of chovanite from Kľačianka, the two compositional types of chovanite were found (Figure 14). The first and more abundant is chovanite with a mean Pb/Sb ratio of 0.90 (0.88–0.93) and  $x$ -value of 0.63 (0.50–0.72), which is very close to the recently studied samples from Dúbrava (Sejkora, *unpublished data*). It locally contains minor amounts of Ag (up to 0.13 *apfu*) and Cl (up to 0.18 *apfu*). The much rarer Pb-rich chovanite was observed only in one sample and has a Pb/Sb ratio of 0.98 (0.97–0.99), mean calculated  $x$ -value was 0.32 (0.28–0.35), and locally also Cl contents up to 0.10 *apfu* were detected. The chemical analyses of chovanite and the corresponding empirical formulae are given in Table S12. Due to the fact that the chemical composition of chovanite from Kľačianka is not so far from the ideal empirical formula  $\text{Pb}_7\text{Sb}_8\text{S}_{19}$  given for heteromorphite [54], we also confirmed its determination by Raman spectroscopy. The experimental spectra of chovanite from Kľačianka (Figure 15) agree very well with spectra of PXRD-confirmed chovanite from Dúbrava and chovanite from Pollone mine, in Italy.

**Semseyite** occurs as an elongated euhedral to subhedral grains up to  $200 \mu\text{m}$  in length in zinkenite aggregates and in their fissures (Figure 4a), in association with jamesonite and robinsonite. It was also observed as grains up to  $10\text{--}20 \mu\text{m}$  integrown with boulangerite to aggregates up to  $100 \mu\text{m}$  across. Chemical analyses of semseyite from Kľačianka (Table S13) correspond to the ideal formula  $\text{Pb}_9\text{Sb}_8\text{S}_{21}$  (Moëlo et al. 2008); the value  $N$  of pligionite homologous series, calculated as  $N = 4\text{Pb}/\text{Sb} - 0.5$  [75], in the range 3.87–4.06 (mean 3.96), is close to ideal value  $N = 4$ . The mean composition of semseyite, calculated from 38 analyses on the base of 38 *apfu*, is  $\text{Pb}_{8.94}\text{Sb}_{8.01}\text{S}_{21.05}$ .

**Boulangerite** was found as grey metallic fibrous aggregates (some with brownish tint) up to 1 cm in quartz gangue. In polished sections, it is usually closely associated with younger rouxelite and dadsonite as euhedral acicular crystals up to  $25\text{--}30 \times 500 \mu\text{m}$  in size

or as anhedral aggregates (Figures 4c and 10a–c). It intergrows with or replaces bournonite. The PXRD data of boulangerite from Kľačianka agree well with published data of this mineral phase and also with the theoretical pattern calculated from the crystal structure information published by Ventruti et al. [76]; its refined unit-cell parameters are given in Table 1. Chemical analyses of boulangerite (Table S14) correspond to ideal formula  $Pb_5Sb_4S_{11}$  [54] (Moëlo et al. 2008) with remarkable contents of Cl up to 0.13 *apfu* (0.24 wt.% Cl). Similar increased Cl contents in boulangerite have not been described yet. Some minor Cl contents are known only in boulangerite from Seravezza, Italy (0.05 wt.% Cl; [71]); Ochtiná—Čížko baňa, Slovakia (up to 0.09 wt.% Cl; [63]); or Prachovice, Czech Republic (up to 0.08 wt.% Cl; [77]). The Cl contents slightly negatively correlates with Sb (Figure 16).

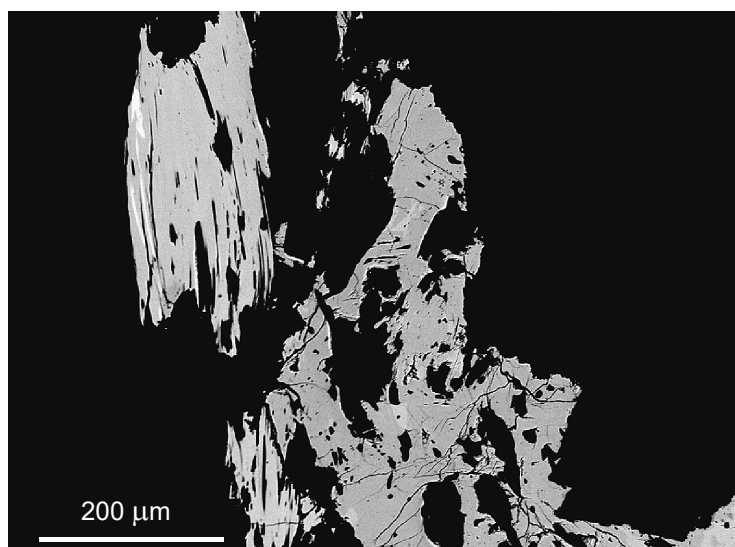


**Figure 13.** Chovanite aggregates (light grey) with relics of boulangerite (white) in association with rouxelite (dark grey). BSE photo.

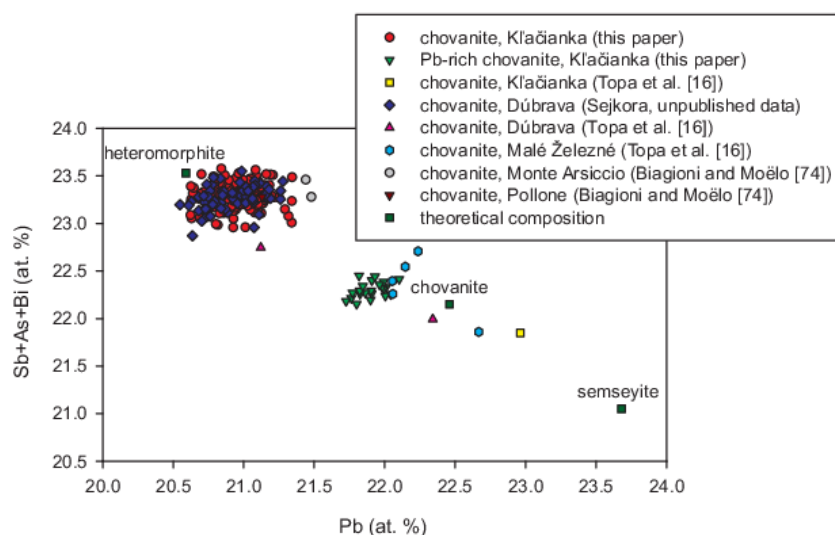


**Figure 14.** Chemical composition of chovanite in the graph Pb vs. Sb + As + Bi (at.%); theoretical composition: heteromorphite  $Pb_7Sb_8S_{19}$ , chovanite  $Pb_{15-2x}Sb_{14+2x}S_{36}O_x$  ( $x = 0.2$ ), and semseyite  $Pb_9Sb_8S_{21}$ ; for Tl-containing samples from Monte Arsiccio and Pollone mines, the  $Pb_{corr}$  and  $Sb_{corr}$  data (Biagioni, Moëlo [74]) are used.

**Geocronite** was determined only rarely in association with boulangerite, robinsonite, jamesonite, and galena. It forms irregular aggregates up to 200  $\mu m$  across in quartz gangue.

Its chemical composition (Table S15) is close to the ideal formula  $\text{Pb}_{14}(\text{Sb,As})_6\text{S}_{23}$  [54]. Contents of As, characteristic for this mineral (solid solution geocronite-jordanite), are in the range of 0.42–1.33 *apfu*. Its empirical formula (mean of eight analyses on the base of 43 *apfu*) is  $\text{Pb}_{13.97}(\text{Sb}_{5.02}\text{As}_{0.85})_{\Sigma 5.87}\text{S}_{23.16}$ .

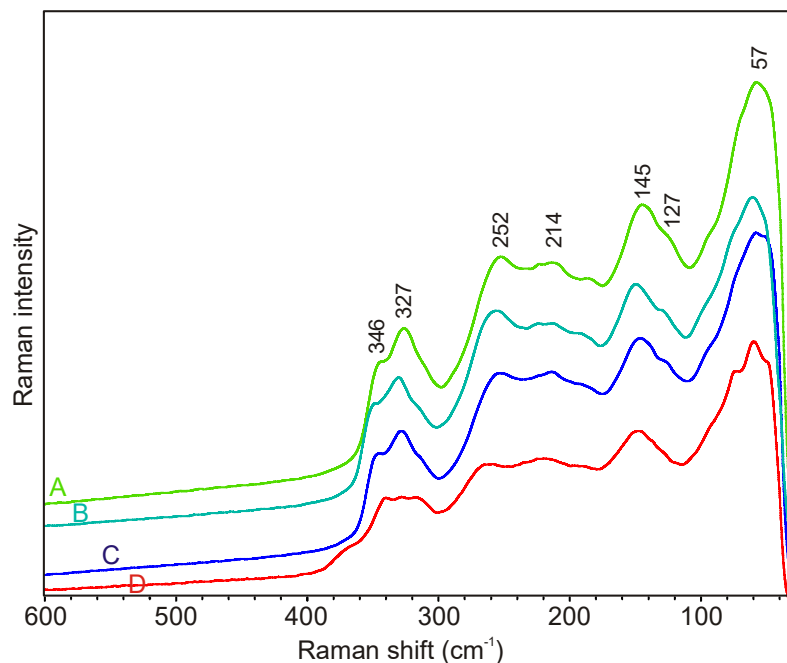


**Figure 15.** Comparison of Raman spectra of chovanite from Kl'áčianka (two samples A and B); Dúbrava deposit; Dimitrij vein (C); and Pollone mine, Italy (D).

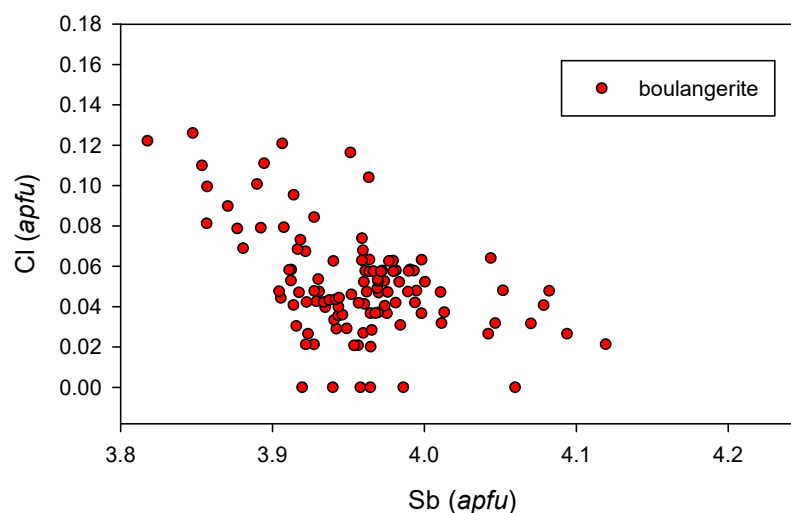


**Figure 16.** The graph of Sb vs. Cl contents (*apfu*) for boulangerite.

#### 4.2. Other Sulphosalts and Gold

**Tetrahedrite-group minerals** form grey metallic aggregates up to 1 cm in size in quartz gangue in association with bournonite and other sulphosalts; some of their aggregates contain inclusions of Sb-rich bismuthinite, Bi-rich chalcostibite, tintinaite, and Cu-bearing robinsonite. Part of the aggregates shows weak chemical zoning due to  $\text{HgFe}_{-1}$  and  $\text{SbAs}_{-1}$  substitutions (Figure 17a,b). They probably form several generations. The PXRD data of tetrahedrite-(Zn) from Kl'áčianka agree well with published data of this mineral phase and also with theoretical patterns calculated from the crystal structure information by Peterson and Miller [78]; its refined unit-cell parameters are given in Table 1. The

chemical composition of tetrahedrite-group members in the studied material is relatively variable (Figures 18–20). According to the recently published nomenclature scheme of minerals of the tetrahedrite group  $(\text{Cu,Ag})_6[\text{Cu}_4(\text{Fe,Zn,Hg})_2](\text{Sb,As})_4\text{S}_{13}$  [79], studied minerals correspond to **tetrahedrite-(Fe)** and **tetrahedrite-(Zn)**, both with some Hg contents (Figure 18). The trigonal position of both members is predominantly occupied by Cu, with minor amounts of Ag (0.03–0.38 *apfu*); increased Ag contents were found especially in the members with low Hg contents (Figure 19). Tetrahedrite-(Fe) shows dominant Fe in the range 0.85–1.28 *apfu* accompanied by Zn (0.27–0.88 *apfu*) and Hg (0.17–0.74 *apfu*). In tetrahedrite-(Zn), Zn is the prevailing element (ranging between 0.85 and 1.45 *apfu*); Fe and Hg contents are in the range 0.44–0.88 and 0.06–0.33 *apfu*, respectively. For both minerals, Sb is considerably prevailing (2.57–4.01 *apfu*) over As (0.01–1.32 *apfu*), and Bi contents are negligible (up to 0.09 *apfu*). Increased As contents were observed in the Fe- and Hg-rich members (Figure 20). Chemical analyses of tetrahedrite-group minerals and the corresponding empirical formulae are given in Table S16. The observed variability of the chemical composition of tetrahedrite indicates different formation conditions in individual veins.

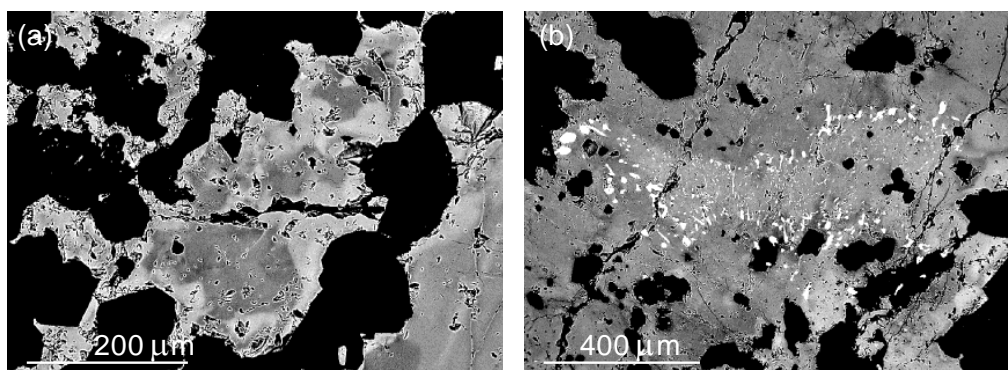


**Figure 17.** (a) Zonality of tetrahedrite-(Fe) due to  $\text{HgFe}_{-1}$  and  $\text{SbAs}_{-1}$  substitutions; (b) bismuthinite inclusions (white) in zonal tetrahedrite-(Fe). BSE photos.

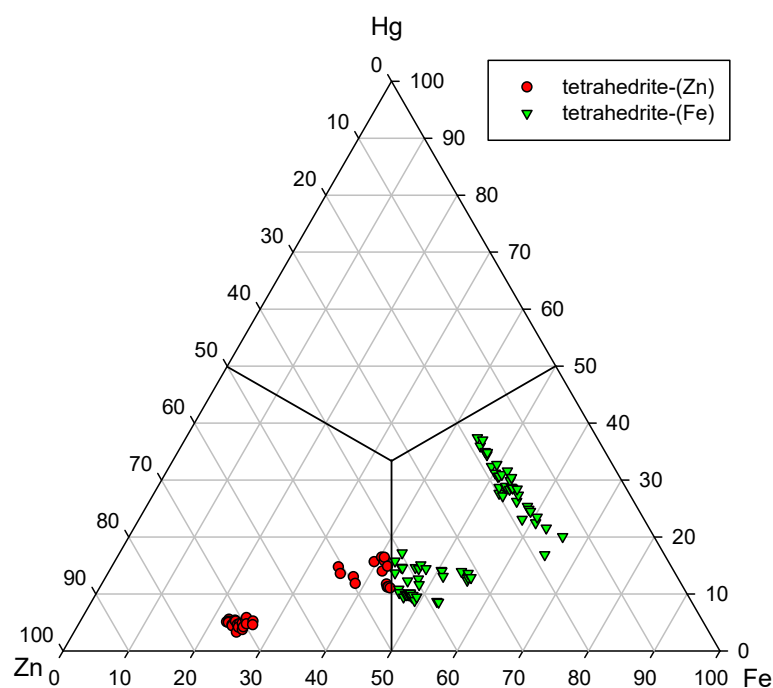


**Figure 18.** Ternary plot Fe–Hg–Zn (*apfu*) for members of the tetrahedrite group.

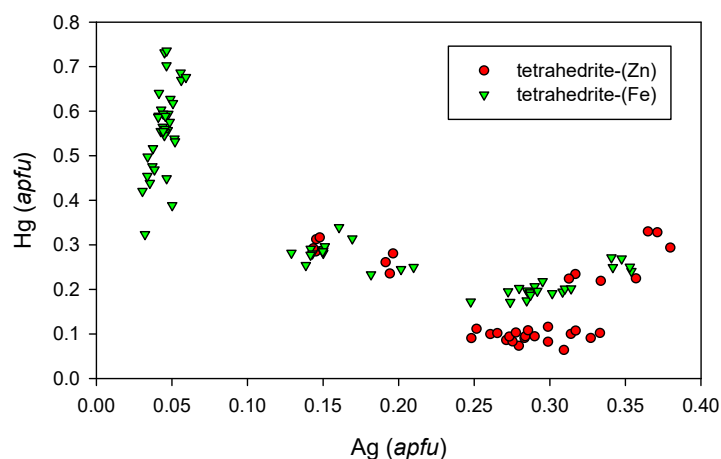


Figure 19. Chemical composition of the tetrahedrite group minerals in the graph Ag vs. Hg (*apfu*).

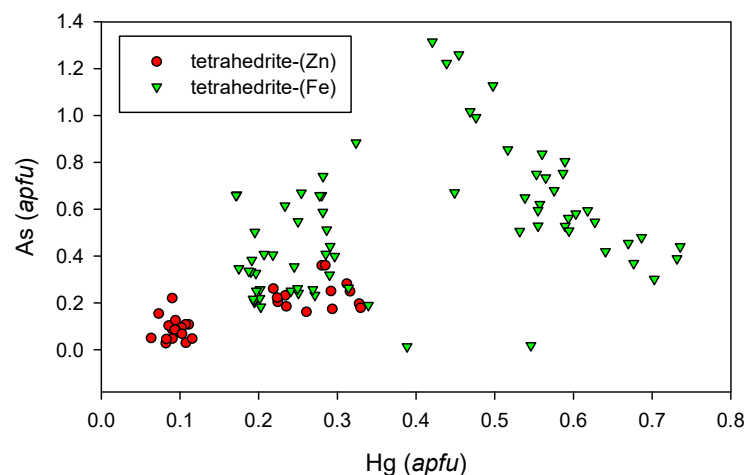
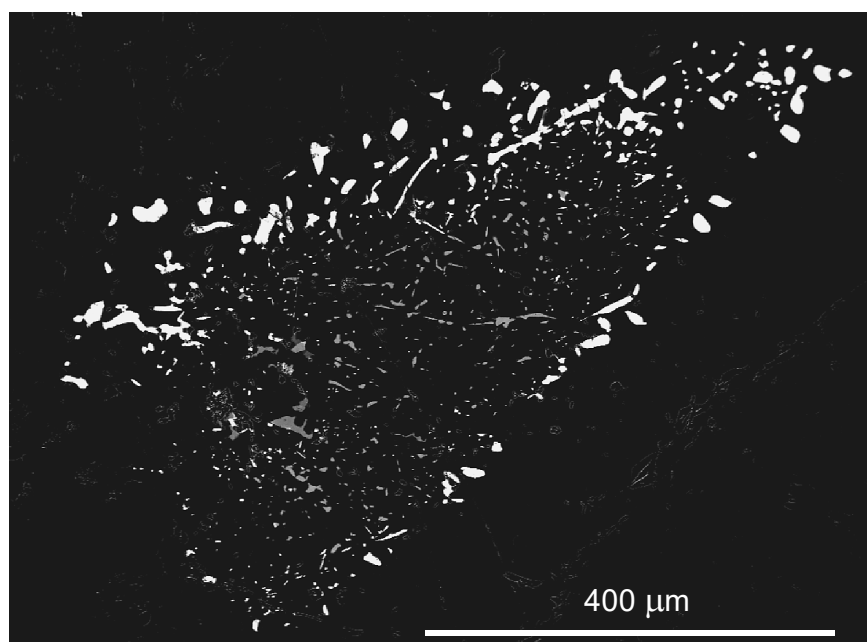


Figure 20. Chemical composition of the tetrahedrite group minerals in the graph Hg vs. As (*apfu*).

**Bournonite** occurs as massive grey metallic aggregates up to 0.5 cm size in quartz gangue. In polished sections, it is associated with boulangerite, rouxelite, and dadsonite (Figure 10b) or forms inclusions (with tintinaite or Cu-bearing robinsonite) up to 300  $\mu\text{m}$  in size in tetrahedrite (Figure 5a–b). The chemical composition of bournonite from Kľáčianka (Table S17) is nearly stoichiometric, with As contents reaching only up to 0.04 *apfu* and locally present very minor amounts of Ag and Bi (up to 0.01 *apfu*). Its empirical formula (mean of 56 analyses on the base of 6 *apfu*) is  $\text{Pb}_{0.99}\text{Cu}_{1.01}(\text{Sb}_{1.00}\text{As}_{0.01})_{\Sigma 1.01}\text{S}_{2.99}$ .

**Chalcostibite** forms irregular dark grey metallic aggregates up to 0.5 cm in size in quartz gangue, in association with stibnite, jamesonite, and zinkenite. Its PXRD data agree well with published data of this mineral phase and also with the theoretical pattern calculated from the crystal structure information by Kiono, Kimata [80]; its refined unit-cell parameters are given in Table 1. Chemical analyses of chalcostibite (Table S18) correspond to the ideal composition of this mineral and its empirical formula (mean 14 analyses on the base of four *apfu*) is  $\text{Cu}_{0.99}\text{Sb}_{1.01}\text{S}_{2.00}$ .

An unusual **Bi-rich chalcostibite** (a member of chalcostibite-emplactite solid solution) was observed as a subhedral inclusion and more rarely as acicular crystals up to 80  $\mu\text{m}$  in tetrahedrite-(Fe) in association with Sb-rich bismuthinite (Figure 21). It contains 0.28–0.33 *apfu* of Bi and its chemical composition (Table S18) corresponds to the following empirical formula:  $\text{Cu}_{1.05}(\text{Sb}_{0.66}\text{Bi}_{0.33})_{\Sigma 0.96}\text{S}_{1.99}$  (mean of 11 analyses).



**Figure 21.** The inclusions of Bi-rich chalcostibite (grey) and Sb-rich bismuthinite (white) in tetrahedrite-(Fe) (black). BSE photo.

**Stibnite** belongs to the most abundant ore minerals in the studied material; it forms fine-grained aggregates up to 10 cm in size and also elongated lath-like crystals up to 3 cm in length enclosed in quartz gangue. It is usually associated with zinkenite. The PXRD data of stibnite from Kl'áčianka agree well with the published data of this mineral phase and also with the theoretical pattern calculated from the crystal structure information by Kyono, Kimata [81]; its refined unit-cell parameters are given in Table 1. The chemical composition of stibnite (Table S19) is close to its ideal stoichiometry  $Sb_2S_3$  without the presence of any minor elements.

**Bismuthinite** forms rare subhedral, oval to elongated grains up to 60  $\mu m$  in size in tetrahedrite aggregates (Figure 17b), sometimes in association with Bi-rich chalcostibite (Figure 21). Increased contents of Sb in ideal formula  $(Bi,Sb)_2S_3$  in the range 0.15–0.75 *apfu* as well as minor contents of Pb and Cu are characteristic. The determined Cu contents (mean 0.13, range 0.05–0.25 *apfu*) are significantly higher than the Pb contents (0.02; 0.01–0.05 *apfu*); this indicates that Cu enters this crystal structure by a different type of substitution than the usual aikinite one or possible influence/incorporation of Cu from surrounding tetrahedrite. Chemical analyses of bismuthinite and corresponding empirical formulae are given in Table S20.

**Gladite** was observed only rarely as irregular anhedral grains up to 30  $\mu m$  across in pyrite in association with tetrahedrite-(Fe) with inclusions of Sb-rich bismuthite and Bi-rich chalcostibite. The chemical composition of this member of bismuthinite-aikinite solid solution is shown in Table S21. The value of  $n_{aik}$  (calculated according Topa et al. [82]) ranged between 29.4 and 36.7. The presence of Sb (up to 0.48 *apfu*) substituting for Bi is a characteristic feature of gladite from Kl'áčianka. Minor contents of Fe were also detected and are probably influenced by the surrounding pyrite. The mean composition of gladite (calculated from seven analyses on the base of 16 *apfu*) is  $Cu_{1.02}Pb_{1.00}Fe_{0.23}(Bi_{4.38}Sb_{0.41})_{\Sigma 4.79}S_{8.95}$ .

**Gold** was observed only rarely as oval inclusions up to 10  $\mu m$  in size enclosed in tetrahedrite aggregates, in association with Sb-rich bismuthinite and Bi-rich chalcostibite. It contains minor amounts of Ag (0.07–0.12 *apfu*), Hg (0.01–0.03 *apfu*), and Cu (0.03–0.05 *apfu*); increased totals of analyses (Table S22) may indicate the origin of Cu contents from surrounding tetrahedrite.

#### 4.3. Associated Sulphides

**Pyrite** is an abundant constituent of quartz gangue at the studied locality, but it is rare in the samples with sulphosalts. It forms aggregates up to 0.5 cm in size and occasionally also euhedral crystals up to 1 mm across. The chemical composition of pyrite from Kl'áčianka corresponds to the ideal formula, with As contents only up to 0.02 *apfu* as well as very minor amounts of Sb (up to 0.01 *apfu*) and Pb (up to 0.002 *apfu*). Its chemical analyses and corresponding empirical formulae are given in Table S23.

**Arsenopyrite** is a relatively rare component of quartz gangue, usually in association with pyrite. It occurs as fine-grained aggregates up to 100  $\mu\text{m}$  in size. During the study of its chemical composition (Table S24), we observed only the major elements and its distinct As-poor character. The determined range of  $\text{AsS}_{-1}$  substitution (1.16–1.20 *apfu* S) is slightly larger than published by Kretschmar and Scott [83] or Sharp et al. [84] but corresponds to the composition of arsenopyrite from e.g., gold deposits [85,86] or the S-richest arsenopyrite from nearby Dúbrava deposit [41]. The mean composition of arsenopyrite (calculated from seven analyses on the base of 3 *apfu*) is  $\text{Fe}_{1.00}\text{As}_{0.82}\text{S}_{1.18}$ .

**Sphalerite** is relatively abundant in samples with sulphosalts. It forms irregular aggregates and grains up to 3 mm in size. The two types of sphalerite were distinguished based on chemical composition. The first one is Cd-bearing with up to 0.73 wt.% of Cd (0.006 *apfu*), 0.44 wt.% of Fe (0.008 *apfu*), and only locally containing also 0.63 wt.% of Hg (0.003 *apfu*). The second one is a Hg-bearing variety with Hg contents reaching up to 1.71 wt.% (0.008 *apfu*) and with 0.50 wt.% of Fe (0.009 *apfu*), which is Cd-free. Chemical analyses of both types of sphalerite and corresponding empirical formulae are given in the Table S25.

**Galena** occurs as rare microscopic anhedral grains and veinlets up to 100  $\mu\text{m}$  in the aggregates of sulphosalts. It was also observed as black weathered aggregates up to several mm in size partly replaced by supergene anglesite in quartz gangue. The chemical composition of galena from Kl'áčianka is nearly stoichiometric, only with minor Sb contents up to 0.02 *apfu*. Its chemical analyses and corresponding empirical formulae are given in Table S26.

#### 5. Discussion and Conclusions

Reconstruction of a crystallization sequence of sulphosalts/ore minerals at Kl'áčianka is complicated due to several facts: (i) studied samples very probably come from several independent hydrothermal veins, each containing a partly different mineral association; (ii) missing mutual contacts among some of the ore minerals; (iii) isolated multicomponent sulphosalts aggregates with contrasting mineral compositions typically contain only a restricted number of ore minerals; (iv) simple chemistry of some phases (bournonite, galena, jamesonite) vs. very variable composition of others (e.g., minerals of tetrahedrite group) preclude the check for possible presence of their multiple generations.

However, on the basis of detailed observation of hand-specimens, ore microscopy, and BSE images, we can propose a following sequence of crystallization of studied ore mineralization: (i) pyrite and arsenopyrite; (ii) earlier sulphosalt assemblage—stibnite, zinkenite, robinsonite; (iii) middle-stage sulphosalt assemblage—jamesonite, boulangerite, chalcostibite, bournonite; probably scainiite, geocronite, and semseyite; as well as probably part of tetrahedrite; (iv) younger sulphosalt assemblage—with typical sequence: rouxelite  $\rightarrow$  dadsonite  $\rightarrow$  chovanite  $\rightarrow$  disulfodadsonite; (v) tetrahedrite with inclusions of bournonite, tintinaite, Sb-rich bismuthinite, Bi-rich chalcostibite, gold, and Cu-bearing robinsonite. The time evolution of mineralization stages (i)–(iv) is quite clear and well documented. Their relation to (v), however, is not easy to discern because in studied samples, tetrahedrite (v) is rare and does not occur in association with Pb–Sb sulphosalts.

The observed sulphosalts assemblages (ii)–(iv) from Kl'áčianka correspond very well to stibnite–sphalerite–Pb–Sb sulfosalts stage defined at nearby Dúbrava antimony deposit [42], which is well documented also at a number of other localities in this area [41,45]. This mineral stage at the Dúbrava deposit originated from aqueous fluids (with NaCl–KCl,

below halite saturation), with traces or without CO<sub>2</sub>, and homogenization temperature of 105–170 °C, but fluid inclusions in stibnite and some populations in quartz show lower salinities [41,42]. The age of this stage (determined by U/Pb dating in hydrothermal carbonates) scatters around 322 Ma, showing that this mineralization is late Variscan [45].

The assemblage of tetrahedrite with inclusions of Pb–(Cu)–Sb–Bi sulphosalts at Kl'áčianka is practically identical with the “tetrahedrite (PbSbBi sulphosalts) stage” developed at Dúbrava deposit and defined by Chovan et al. [42] or the “dolomite-baryte-tetrahedrite stage” of Majzlan et al. [41,45]. Aqueous fluid inclusions in quartz of this stage from the Dúbrava deposit yielded homogenisation temperatures of 108–157 °C and salinities mostly between 1 and 14 wt.% NaCl eq. [42]. The U/Pb dating of the hydrothermal dolomite–ankerite associated with quartz and tetrahedrite gave two groups of ages. One of them averaging around 144 Ma, in the lowermost Cretaceous; the second group (probably representing remobilization) is much younger, of Miocene age [45].

The chlorine-rich character of the studied mineral association at Kl'áčianka is its characteristic phenomenon. It is represented not only by the Cl-sulphosalt and dadsonite, but increased Cl contents were observed in all sulphosalts whose crystal structures allow the incorporation of Cl (boulangerite, chovanite, disulfodadsonite, robinsonite, rouxelite, scainiite, or tintinaite). Such high concentrations of Cl in these sulphosalts are generally rare and are so far the highest known worldwide. These observations indicate the elevated chlorine activity in the ore-forming fluids at some stage.

Another notable feature of the mineral association at Kl'áčianka is the presence of oxygen-containing sulphosalts (rouxelite, scainiite, and chovanite), which clearly required elevated oxygen fugacity in hydrothermal fluids. Their interpretation as products of mixing with an oxidised, low-temperature, perhaps meteoric fluids [41], is questionable due to the presence of elevated Cl contents in studied phases, which suggests simultaneous increase chlorine and oxygen activity in the hydrothermal fluids. A separate question is the presence of rare disulfodadsonite, which requires a high value of sulphur fugacity for its formation [69] or, perhaps, a raised oxidation potential, which would cause a partial change from the S<sup>2-</sup> regime to the S<sup>0</sup> situation with ensuing polymerization of sulphur.

It is obvious that the very specific conditions (elevated O<sub>2</sub>/S<sub>2</sub> fugacity) and high chlorine activity in ore-forming fluids were necessary for the crystallization of the rare chloro-, oxy- and oxy-chloro-sulphosalts at the studied locality. In addition to similar localities in the Nízke Tatry Mts. (Dúbrava—in particular the Dimitrij vein, Malé Železné or Rišianka), the occurrence of analogous associations of Cl and O-bearing sulphosalts is known only from a few localities in Apuan Alps, especially from the Buca della Vena mine [14,57,59], the Polone mine, or Seravezza marbles in Italy [69].

**Supplementary Materials:** The following are available online at <https://www.mdpi.com/article/10.3390/min11091002/s1>, Table S1: Electron probe microanalyses—the analytical conditions, standards and used X-ray lines, Table S2: Chemical composition of zinkenite, Table S3: Chemical composition of scainiite, Table S4: Chemical composition of jamesonite, Table S5: Chemical composition of robinsonite, Table S6: Chemical composition of tintinaite, Table S7: Chemical composition of disulfodadsonite, Table S8: X-ray powder diffraction pattern of dadsonite, Table S9: Chemical composition of dadsonite, Table S10: X-ray powder diffraction pattern of rouxelite, Table S11: Chemical composition of rouxelite, Table S12: Chemical composition of chovanite, Table S13: Chemical composition of semseyite, Table S14: Chemical composition of boulangerite, Table S15: Chemical composition of geocronite, Table S16: Chemical composition of tetrahedrite-group minerals, Table S17: Chemical composition of bournonite; Table S18: Chemical composition of chalcostibite, Table S19: Chemical composition of stibnite, Table S20: Chemical composition of bismuthinite, Table S21: Chemical composition of gladite, Table S22: Chemical composition of gold, Table S23: Chemical composition of pyrite, Table S24: Chemical composition of arsenopyrite, Table S25: Chemical composition of sphalerite, Table S26: Chemical composition of galena.

**Author Contributions:** J.S. and M.Š. conceived and designed the study, with J.P. and R.H. provided field works and found the mineralogical samples. J.S., J.P. and R.H. conducted the WDS analyses; J.S. the X-ray powder diffraction and Raman spectroscopy studies. J.S., E.M. and M.C. interpreted the

results. J.S., M.Š. and J.P. wrote the paper. All authors have read and agreed to the published version of the manuscript.

**Funding:** The research was financially supported by the Ministry of Culture of the Czech Republic (long-term project DKRVO 2019-2023/1.II.c; National Museum, 00023272).

**Data Availability Statement:** The data presented in this study are available in the Supplementary Materials.

**Acknowledgments:** The authors thank Bohuslav Bureš (Praha) and Miroslav Zeman (Jičín) for their kind help with the field works; Cristian Biagioni (Università di Pisa) for loan of type material of Italian sulphosalts; and Radek Škoda (Masaryk University, Brno), Daniel Ozdín (Comenius University, Bratislava), Zdeněk Dolníček and Jana Ulmanová (National Museum, Praha) for their kind help with the analytical work. We must also thank Jiří Litochleb (deceased, National Museum, Praha) for his cooperation in ore microscopy and succession studies. Authors also wish to thank Juraj Majzlan (Friedrich-Schiller-Universität, Jena) for valuable discussion, which helped to improve the quality of manuscript. Referees as well as academic editors are acknowledged for comments and suggestions that helped to improve the early version of the manuscript.

**Conflicts of Interest:** The authors declare no conflict of interest.

## References

- Hak, J. Mineralogy and geochemistry of the Nízke Tatry Sb deposits. *Sbor. Geol. Věd Geol.* **1966**, *7*, 71–144. (In Czech)
- Ralbovský, E. Other occurrences of chalcostibite in the northwestern part of the Nízke Tatry Mts. *Mineral. Slovaca*. **1976**, *8*, 273–278. (In Slovak)
- Chovan, M.; Póč, I.; Jancsy, P.; Majzlan, J.; Krištín, J. Sb-Au(As-Pb) mineralization of the Magurka deposit, Nízke Tatry Mts. *Mineral. Slovaca*. **1995**, *27*, 397–406. (In Slovak)
- Chovan, M.; Slavkay, M.; Michálek, J. Metallogeny of the Ďumbierské Tatry Mts., Western Carpathians. *Mineral. Slovaca*. **1998**, *30*, 3–9. (In Slovak)
- Majzlan, J.; Chovan, M.; Michálek, J. Ore occurrences at Rišianka and Malé Železné—mineralogy and assemblages. *Mineral. Slovaca*. **1998**, *30*, 52–59. (In Slovak)
- Bakos, F.; Chovan, M.; Michálek, J. Mineralogy of hydrothermal Sb, Cu, Pb, Zn, As mineralization in NE of the Magurka deposit, Nízke Tatry Mts. *Mineral. Slovaca*. **2000**, *32*, 497–506. (In Slovak)
- Pršek, J. Chemical Composition and Crystallochemistry of Sulfoalloys from the Hydrothermal Mineralizations from Western Carpathians. PhD. Thesis, Comenius University Bratislava, Bratislava, Slovakia, 2004; pp. 1–135. (In Slovak)
- Lalinská, B.; Chovan, M. Hydrothermal mineralization at localities Medzibrod and Sopotnická dolina. *Mineral. Slovaca*. **2006**, *38*, 261–272. (In Slovak)
- Smirnov, A.; Pršek, J.; Chovan, M. Mineralogy and geochemistry of the Nižná Boca Sb-Au hydrothermal ore deposit (Western Carpathians). *Mineralogia* **2006**, *38*, 71–94. [[CrossRef](#)]
- Majzlan, J.; Števko, M.; Chovan, M. Mineralogy of an ore occurrence near Hiadel' in the Nízke Tatry Mts. (Slovakia). *Bull. Mineral. Petrolog. Odd. Nár. Muz.* **2015**, *24*, 271–276. (In Slovak)
- Mikuš, T.; Bakos, F.; Števko, M. New data on Au mineralization at the Medzibrod locality (Nízke Tatry Mts.), Slovak Republic. *Bull. Mineral. Petrolog.* **2018**, *26*, 154–162. (In Slovak)
- Čík, Š.; Chovan, M.; Majzlan, J. Occurrences of hydrothermal Sb–Au mineralization at Lomnistá, Husárka and Suchá dolina near Jasenie (Nízke Tatry Mts.). *Bull. Mineral. Petrolog.* **2020**, *28*, 210–218. (In Slovak) [[CrossRef](#)]
- Ralbovský, E.; Krištín, J. Occurrence of horobetsuite (Bi,Sb)<sub>2</sub>S<sub>3</sub> at the deposit Dúbrava. *Geol. Sbor. Geol. Carpath.* **1975**, *26*, 141–148.
- Orlandi, P.; Meerschaut, A.; Moëlo, Y.; Palvadeau, P.; Leone, P. Lead–antimony sulfosalts from Tuscany (Italy). VIII. Rouxelite, Cu<sub>2</sub>HgPb<sub>22</sub>Sb<sub>28</sub>S<sub>64</sub>(O,S)<sub>2</sub>, a new sulfosal salt from Buca della Vena mine, Apuan Alps: Definition and crystal structure. *Can. Mineral.* **2005**, *43*, 919–933. [[CrossRef](#)]
- Makovicky, E.; Topa, D.; Mumme, W.G. The crystal structure of dadsonite. *Can. Mineral.* **2006**, *44*, 1499–1512. [[CrossRef](#)]
- Topa, D.; Sejkora, J.; Makovicky, E.; Pršek, J.; Ozdín, D.; Putz, H.; Dittrich, H.; Karup-Møller, S. Chovanite, Pb<sub>15-2x</sub>Sb<sub>14+2x</sub>S<sub>36</sub>O<sub>x</sub> (x ~ 0.2), a new sulphosal salt species from the Low Tatra Mountains, Western Carpathians, Slovakia. *Eur. J. Mineral.* **2012**, *24*, 727–740. [[CrossRef](#)]
- Jakeš, P. Contribution to the Knowledge of Stibnite Veins at the Dúbrava Deposit in the Nízke Tatry Mts. Master's Thesis, Charles University, Prague, Czech Republic, 1962; pp. 1–109. (In Czech)
- Bakos, F. Mineralogy of the Hydrothermal Mineralization NE of Magurka (Nízke Tatry Mts.). Master's Thesis, Comenius University, Bratislava, Slovakia, 1998; pp. 1–100. (In Slovak)
- Pršek, J.; Ozdín, D. Chemical composition of the sulphosalts from the bismuthinite-aikinite series from Western Carpathians. *Acta Miner.-Petrogr. Abstr. Ser.* **2006**, *5*, 100.
- Chovan, M.; Pršek, J.; Klimko, T. Bi sulphosalts from the antimony mineralization (Western Carpathians). *Mineral. Spec. Pap.* **2008**, *32*, 51.

21. Hovorič, R. Characteristics of the Sb Mineralization from the Malé Železné and Kl'áčianka Localities. Master's Thesis, Faculty of Natural Sciences, Comenius University, Bratislava, Slovakia, 2008; pp. 1–110, unpublished (In Slovak)
22. Makovicky, E.; Topa, D. The crystal structure of sulfosalts with boxwork architecture and their new representative,  $Pb_{15-2x}Sb_{14+2x}S_{36}O_x$ . *Can. Mineral.* **2009**, *47*, 3–24. [[CrossRef](#)]
23. Sejkora, J.; Ozdín, D.; Laufek, F.; Plášil, J.; Litochleb, J. Marrucciite, a rare Hg-sulfosalts from the Gelnica ore deposit (Slovak Republic), and its comparison with the type occurrence Buca della Vena mine (Italy). *J. Geosci.* **2011**, *56*, 399–408. [[CrossRef](#)]
24. Števko, M.; Sejkora, J.; Dolníček, Z.; Škácha, P. Selenium-rich Ag–Au mineralization at the Kremnica Au–Ag epithermal deposit, Slovak Republic. *Minerals* **2018**, *8*, 572. [[CrossRef](#)]
25. Števko, M.; Sejkora, J. Bismuth, lead-bismuth and lead-antimony sulphosalts from the granite-hosted hydrothermal quartz veins at the Elisabeth mine, Gemerská Poloma, Spišsko-gemerské rudohorie Mts., Slovakia. *J. Geosci.* **2021**, in print.
26. Pršek, J.; Ozdín, D.; Sejkora, J. Eclarite and associated Bi sulfosalts from the Brezno-Hviezda occurrence (Nízke Tatry Mts, Slovak Republic). *N. Jb. Mineral. Abh.* **2008**, *185*, 117–130. [[CrossRef](#)]
27. Števko, M.; Sejkora, J.; Peterec, D. Grumiplucite from the Rudňany deposit, Slovakia: A second world-occurrence and new data. *J. Geosci.* **2015**, *60*, 269–281. [[CrossRef](#)]
28. Sejkora, J.; Buixaderas, E.; Škácha, P.; Plášil, J. Micro-Raman spectroscopy of natural members along  $CuSbS_2$ – $CuSbSe_2$  join. *J. Raman Spectrosc.* **2018**, *49*, 1364–1372. [[CrossRef](#)]
29. Sombathy, L. *Report on Archive Research of the Antimony Deposit Dúbrava and its Surroundings, the Nízke Tatry Mts*; Geofond: Bratislava, Slovakia, 1969; pp. 1–232, unpublished report. (In Slovak)
30. Lisý, E. *The Nízke Tatry Mts.—Mineral Exploration, Prospecting, Annual Report*; Geofond: Bratislava, Slovakia, 1957; pp. 1–18, unpublished report. (In Slovak)
31. Kubíny, D. (Ed.) *Slovensko Sb—Study*; Geofond: Bratislava, Slovakia, 1971; pp. 1–220, unpublished report. (In Slovak)
32. Lehotský, I. *Partial Final Report of the Geological Research of Tatric Crystalline Complex in the Nízke Tatry Mts*; Geofond: Bratislava, Slovakia, 1973; pp. 1–74, unpublished report. (In Slovak)
33. Michálek, J. *Final Report the Nízke Tatry Mts. (11740064)*; Geofond: Bratislava, Slovakia, 1988; pp. 1–237, unpublished report. (In Slovak)
34. Biely, A. (Ed.) *Geological Map of the Nízke Tatry Mts. 1:50 000*; SGÚ-GÚDŠ: Bratislava, Slovakia, 1992.
35. Krist, E.; Korikovskij, S.P.; Putiš, M.; Janák, M.; Faryad, S.W. Geology and Petrology of Metamorphic Rocks of the Western Carpathian Crystalline Complexes. Comenius University Press: Bratislava, Slovakia, 1992; pp. 1–324.
36. Petřík, I.; Broska, I.; Uher, P. Evolution of the Western Carpathian granite magmatism: Age, source rock, geotectonic setting and relation to the Variscan structure. *Geol. Carpath.* **1994**, *45*, 283–291.
37. Biely, A.; Bezák, V. (Eds.) *Explanations of the geological map of the Nízke Tatry Mts. 1:50,000*; Vyd. D. Štúra. GSSR: Bratislava, Slovakia, 1997; pp. 1–232.
38. Kohút, M. Genetic aspects of the Nízke Tatry Mts. granitic rocks genesis. *Mineral. Slovaca.* **1998**, *30*, 83–84. (In Slovak)
39. Chovan, M.; Háber, M.; Jeleň, S.; Rojkovič, I. (Eds.) *Ore Textures in the Western Carpathians*; Slovak Academic Press: Bratislava, Slovakia, 1994; pp. 1–219.
40. Chovan, M.; Slavkay, M.; Michálek, J. Ore mineralizations of the Ďumbierské Tatry Mts. (Western Carpathians, Slovakia). *Geol. Carpath.* **1996**, *47*, 371–382.
41. Majzlan, J.; Chovan, M.; Hurai, V.; Luptáková, J. Hydrothermal mineralisation of the Tatric Superunit (Western Carpathians, Slovakia): I. A review of mineralogical, thermometry and isotope data. *Geol. Carpath.* **2020**, *71*, 85–112.
42. Chovan, M.; Hurai, V.; Sachan, H.K.; Kantor, J. Origin of the fluids associated with granodiorite-hosted, Sb-As-Au-W mineralisation at Dúbrava (Nízke Tatry Mts., Western Carpathians). *Miner. Depos.* **1995**, *30*, 48–54. [[CrossRef](#)]
43. Chovan, M.; Majzlan, J.; Ragan, M.; Siman, P.; Krištín, J. Pb-Sb and Pb-Sb-Bi sulfosalts and associated sulphides from Dúbrava antimony deposit, Nízke Tatry Mts. *Acta Geol. Univ. Comen.* **1998**, *53*, 37–49.
44. Michálek, J.; Chovan, M. Structural-geological and mineralogical evaluation of the Sb deposit Dúbrava. *Mineral. Slovaca.* **1998**, *30*, 25–35. (In Slovak)
45. Majzlan, J.; Chovan, M.; Kiefer, S.; Gerdes, A.; Kohút, M.; Siman, P.; Konečný, P.; Števko, M.; Finger, F.; Waitzinger, M.; et al. Hydrothermal mineralisation of the Tatric Superunit (Western Carpathians, Slovakia): II. Geochronology and timing of mineralisations in the Nízke Tatry Mts. *Geol. Carpath.* **2020**, *71*, 113–133.
46. Sejkora, J.; Števko, M. Scainiite and associated sulphosalts from the Dimitrij vein, Dúbrava Sb deposit, Slovakia. *Minerals* in preparation.
47. Michálek, J. Geological setting and ore mineralization in the surroundings of the Magurka deposit. *Mineral. Slovaca.* **1998**, *30*, 44–51.
48. Ondruš, P. ZDS—A computer program for analysis of X-ray powder diffraction patterns. *Mater. Sci. Forum* **1993**, *133–136*, 297–300, EPDIC-2, Enchede. [[CrossRef](#)]
49. Burnham, C.W. Lattice constant refinement. *Carnegie Inst. Wash. Yearb.* **1962**, *61*, 132–135.
50. Yvon, K.; Jeitschko, W.; Parthé, E. Lazy Pulverix, a computer program for calculation X-ray and neutron diffraction powder patterns. *J. Appl. Cryst.* **1977**, *10*, 73–74. [[CrossRef](#)]
51. Pouchou, J.L.; Pichoir, F. “PAP” ( $\varphi\rho Z$ ) procedure for improved quantitative microanalysis. In *Microbeam Analysis*; Armstrong, J.T., Ed.; San Francisco Press: San Francisco, CA, USA, 1985; pp. 104–106.

52. Portheine, J.C.; Nowacki, W. Refinement of the crystal structure of zinckenite,  $Pb_6Sb_{14}S_{27}$ . *Zeit. Kristallogr.* **1975**, *141*, 79–96.
53. Biagioni, C.; Bindi, L.; Moëlo, Y. Another step toward the solution of the real structure of zinckenite. *Zeit. Kristallogr.* **2018**, *233*, 269–277. [[CrossRef](#)]
54. Moëlo, Y.; Makovicky, E.; Mozgova, N.N.; Jambor, J.L.; Cook, N.; Pring, A.; Paar, W.; Nickel, E.H.; Graeser, S.; Karup-Møller, S.; et al. Sulfosalts Systematics: A Review Report of the Sulfosalt Sub-Committee of the IMA Commission on Ore Mineralogy. *Eur. J. Mineral.* **2008**, *20*, 7–46. [[CrossRef](#)]
55. Moëlo, Y. Contribution à l'étude des conditions naturelles de formation des sulfures complexes d'antimoine et plomb (Sulfosels de Pb/Sb): Signification métallogénique. *Doc. Du BRGM* **1983**, *55*, 1–256.
56. Nikolaev, Y.N.; Prokof'ev, V.Y.; Apletalin, A.V.; Vlasov, E.A.; Baksheev, I.A.; Kal'ko, I.A.; Komarova, Y.S. Gold-telluride mineralization of the Western Chukchi Peninsula, Russia: Mineralogy, geochemistry, and formation conditions. *Geol. Ore Depos.* **2013**, *55*, 96–124. [[CrossRef](#)]
57. Orlandi, P.; Moëlo, Y.; Meerschaut, A.; Palvadeau, P. Lead-antimony sulfosalts from Tuscany (Italy); I. Scainiite,  $Pb_{14}Sb_{30}S_{54}O_5$ , the first Pb-Sb oxy-sulfosalt, from Buca della Vena Mine. *Eur. J. Mineral.* **1999**, *11*, 949–954. [[CrossRef](#)]
58. Moëlo, Y.; Meerschaut, A.; Orlandi, P.; Palvadeau, P. Lead-antimony sulfosalts from Tuscany (Italy) II. Crystal structure of scainiite,  $Pb_{14}Sb_{30}S_{54}O_5$ , an expanded monoclinic derivative of  $Ba_{12}Bi_{24}S_{48}$  hexagonal sub-type (zinckenite group). *Eur. J. Mineral.* **2000**, *12*, 835–846. [[CrossRef](#)]
59. Orlandi, P.; Moëlo, Y.; Meerschaut, A.; Palvadeau, P. Lead-antimony sulfosalts from Tuscany (Italy); III. Pillaite,  $Pb_9Sb_{10}S_{23}ClO_{0.5}$ , a new Pb-Sb chloro-sulfosalt, from Buca della Vena mine. *Eur. J. Mineral.* **2001**, *13*, 605–610. [[CrossRef](#)]
60. Léone, P.; Le Leuch, L.M.; Palvadeau, P.; Molinier, P.; Moëlo, Y. Single crystal structures and magnetic properties of two iron or manganese-lead-antimony sulfides:  $MPb_4Sb_6S_{14}$  (M: Fe, Mn). *Solid State Sci.* **2003**, *5*, 771–776. [[CrossRef](#)]
61. Makovicky, E.; Balić-Žunić, T.; Karanovic, L.; Poleti, D.; Pršek, J. Structure refinement of natural robinsonite,  $Pb_4Sb_6S_{13}$ : Cation distribution and modular description. *N. Jb. Mineral. Mh.* **2004**, 49–67. [[CrossRef](#)]
62. Ayora, C.; Gali, S. Additional data on robinsonite. *Can. Mineral.* **1981**, *19*, 415–417.
63. Števkó, M.; Sejkora, J. Boulangerite and robinsonite from the Ochtiná-Čížko baňa occurrence (Slovak Republic) *Bull. Mineral. Petrolog.* **2017**, *25*, 273–276. (In Slovak)
64. Jambor, J.L.; Lachance, G.R. Bismuthian robinsonite. *Can. Mineral.* **1968**, *9*, 426–428.
65. Zakrzewski, M.A.; Makovicky, E. Izoklakeite from Vena, Sweden, and the kobellite homologous series. *Can. Mineral.* **1986**, *24*, 7–18.
66. Moëlo, Y.; Jambor, J.L.; Harris, D.C. Tintinaite et sulfosels associés de Tintina (Yukon); la cristallographie de la série de la kobellite. *Can. Mineral.* **1984**, *22*, 219–226.
67. Sacharova, M.S.; Krivitskaja, N.N. Mineralogical and geochemical characteristics of Pb-Bi-Sb sulfosalts from gold deposits (Eastern Transbaikal). *Geol. Rud. Mestorožd.* **1970**, *4*, 56–70.
68. Moëlo, Y.; Roger, G.; Maurel-Palacin, D.; Marcoux, E.; Laroussi, A. Chemistry of some Pb-(Cu, Fe)-(Sb, Bi) sulfosalts from France and Portugal. Implications for the crystal chemistry of lead sulfosalts in the Cu-poor part of the  $Pb_2S_2$ - $Cu_2S$ - $Sb_2S_3$ - $Bi_2S_3$  system. *Miner. Petrol.* **1995**, *53*, 229–250. [[CrossRef](#)]
69. Orlandi, P.; Biagioni, C.; Moëlo, Y.; Bonaccorsi, E. Lead-antimony sulfosalts from Tuscany (Italy). XIV. Disulfodadsonite,  $Pb_{11}Sb_{13}S_{30}(S_2)_{0.5}$ , a new mineral from the Ceragiola marble quarry, Apuan Alps: Occurrence and crystal structure. *Eur. J. Mineral.* **2013**, *25*, 1005–1016. [[CrossRef](#)]
70. Cerville, B.D.; Cesbron, F.P.; Sichére, M.C.; Dietrich, J. La chalcostibite et la dadsonite de Saint-Pons, Alpes de Haute Provence, France. *Can. Mineral.* **1979**, *17*, 601–605.
71. Orlandi, P.; Moëlo, Y.; Biagioni, C. Lead-antimony sulfosalts from Tuscany (Italy). X. Dadsonite from the Buca della Vena mine and Bi-rich izoklakeite from the Seravezza marble quarries. *Period. Di Mineral.* **2010**, *79*, 113–121.
72. Moëlo, Y. Quaternary compounds in the system Pb-Sb-S-Cl; dadsonite and synthetic phases. *Can. Mineral.* **1979**, *17*, 595–600.
73. Biagioni, C.; Moëlo, Y.; Orlandi, P. Lead-antimony sulfosalts from Tuscany (Italy). XV. (Tl-Ag)-bearing rouxelite from Monte Arsiccio mine: Occurrence and crystal chemistry. *Mineral. Mag.* **2014**, *78*, 651–661. [[CrossRef](#)]
74. Biagioni, C.; Moëlo, Y. Lead-antimony sulfosalts from Tuscany (Italy). XIX. Crystal chemistry of chovanite from two new occurrences in the Apuan Alps and its 8 Å crystal structure. *Mineral. Mag.* **2017**, *81*, 811–831. [[CrossRef](#)]
75. Makovicky, E. Algorithms for calculations of homologue order N in the homologous series of sulfosalts. *Eur. J. Mineral.* **2019**, *31*, 83–97. [[CrossRef](#)]
76. Ventrucci, G.; Stasi, F.; Pinto, D.; Vurro, F.; Renna, M. The plumose boulangerite from Bottino, Apuan Alps, Italy: Crystal structure, OD character and twinning. *Can. Mineral.* **2012**, *50*, 181–199. [[CrossRef](#)]
77. Sejkora, J.; Smutek, D.; Malíková, R. Sulfide mineralization from the limestone quarry Prachovice, Czech Republic. *Bull. Mineral. Petrolog.* **2017**, *25*, 260–272. (In Czech)
78. Peterson, R.C.; Miller, I. Crystal structure and cation distribution in freibergite and tetrahedrite. *Mineral. Mag.* **1986**, *50*, 717–721. [[CrossRef](#)]
79. Biagioni, C.; George, L.L.; Cook, N.J.; Makovicky, E.; Moëlo, Y.; Pasero, M.; Sejkora, J.; Stanley, C.J.; Welch, M.D.; Bosi, F. The tetrahedrite group: Nomenclature and classification. *Am. Mineral.* **2020**, *105*, 109–122. [[CrossRef](#)]
80. Kyono, A.; Kimata, M. Crystal structures of chalcostibite ( $CuSbS_2$ ) and emplectite ( $CuBiS_2$ ): Structural relationship of stereochemical activity between chalcostibite and emplectite. *Am. Mineral.* **2005**, *90*, 162–165. [[CrossRef](#)]

81. Kyono, A.; Kimata, M. Structural variations induced by difference of the inert pair effect in the stibnite-bismuthinite solid solution series  $(\text{Sb,Bi})_2\text{S}_3$ . *Am. Mineral.* **2004**, *89*, 932–940. [[CrossRef](#)]
82. Topa, D.; Makovicky, E.; Paar, W.H. Composition ranges and exsolution pairs for the members of the bismuthinite–aikinite series from Felbertal, Austria. *Can. Mineral.* **2002**, *40*, 849–869. [[CrossRef](#)]
83. Kretschmar, U.; Scott, S.D. Phase relations involving arsenopyrite in the system Fe-As-S and their application. *Can. Mineral.* **1976**, *14*, 364–386.
84. Sharp, Z.D.; Essene, E.J.; Kelly, W.C. A re-examination of the arsenopyrite geothermometer: Pressure considerations and applications to natural assemblages. *Can. Mineral.* **1985**, *23*, 517–534.
85. Mikulski, S.Z. Te-Bi-Au-Ag-Pb-S mineral assemblages within the late Hercynian polymetallic deposit in the western Sudetes (Poland). In *Guidebook of the International Field Workshop of IGCP-486, Alba Iulia, Romania*; IAGOD: Alba Iulia, Romania, 2004; pp. 242–244.
86. Andráš, P.; Chovan, M. Gold incorporation into sulphide minerals from the Tatric Unit, the Western Carpathians, with respect to their chemical composition. *J. Czech Geol. Soc.* **2005**, *50*, 143–155. [[CrossRef](#)]